Soft Electronic Materials with Combinatorial Properties Generated via Mussel-Inspired Chemistry and Halloysite Nanotube Reinforcement

Pierchala, Malgorzata Karolina; Kadumudi, Firoz Babu; Mehrali, Mehdi; Zsurzan, Tiberiu-Gabriel; Kempen, Paul J; Serdeczny, Marcin Piotr; Spangenberg, Jon; Andresen, Thomas L.; Dolatshahi-Pirouz, Alireza

Published in:
ACS Nano

Link to article, DOI:
10.1021/acsnano.0c09204

Publication date:
2021

Document Version
Peer reviewed version

Soft Electronic Materials with Combinatorial Properties Generated *via* Mussel-Inspired Chemistry and Halloysite Nanotube Reinforcement

Malgorzata Karolina Pierchala,[1] Firoz Babu Kadumudi,[1] Mehdi Mehrali,[1,2,3] Tiberiu-Gabriel Zsurzan,[4] Paul J Kempen,[1] Marcin Piotr Serdeczny,[2] Jon Spangenberg,[2] Thomas L. Andresen,[1,3] Alireza Dolatshahi-Pirouz[1,3,5,*]

[1]Department of Health Technology, Technical University of Denmark, 2800 Kgs. Lyngby, Denmark.

[2]Department of Mechanical Engineering, Technical University of Denmark, 2800 Kgs. Lyngby, Denmark.

[3]Department of Health Technology, Technical University of Denmark, Center for Intestinal Absorption and Transport of Biopharmaceuticals, 2800 Kgs. Lyngby, Denmark.

[4]Department of Electrical Engineering, Technical University of Denmark, 2800 Kgs. Lyngby, Denmark.

[5]Radboud University Medical Center, Radboud Institute for Molecular Life Sciences, Department of Dentistry - Regenerative Biomaterials, Philips van Leydenlaan 25, 6525EX Nijmegen, The Netherlands.

*Correspondence should be addressed to Prof. A. Dolatshahi-Pirouz - aldo@dtu.dk.

Abstract:

Soft and electrically active materials are currently being utilized for intelligent systems, including electronic skin, cybernetics, soft robotics, and wearables. However, fabricating materials that fulfill the highly complex requirements of such advanced applications remains a challenge. These attributes include electronic, adhesive, self-healing, flexible, moldable, printable, and strong mechanical properties. Inspired by the recent interest in transforming mono-functional materials into multifunctional through nanoreinforcement and mussel-inspired chemistry, we have designed a simple two-step methodology based on halloysite nanotubes (HNT) and polydopamine (PDA) to address the grand challenge in the field. In brief, HNTs were coated with PDA and embedded within a polyvinyl alcohol (PVA)-based polymeric matrix in combination with ferric ions (Fe^{3+}). The finalized composite displayed a 3-fold increase in electrical conductivity, a 20-fold increase in mechanical stiffness, and a 7-fold increase in energy dissipation compared to their non-functional counterparts; something that arose from a combination of nanotube alignment and mussel-inspired chemistry. Moreover, the developed composite could elongate up to 30000% of its original length, maintain its electrical properties up to 600% strain, self-heal within seconds (both electrically and mechanically), and displayed strain-sensitivity. Finally, it was 3D-printable, and thus amenable for engineering of customized wearable electronics.

Keywords: self-healing; hydrogels; flexible electronics; nanomaterials; halloysite nanotubes, healthcare monitoring; 3D printing.

Over the past decades, advanced materials have evolved significantly and influenced our society and its citizens. However, today, it is no longer enough that materials are advanced and functional; they also need to be smart and adaptive in an almost animated manner. Such intelligent and vivid materials are typically achieved by tapping into the realm of electromagnetism in one way or another. Examples of their applications are virtually limitless and expanding rapidly. Especially, soft electronic materials capable of bridging the gap between living matter and conventional circuits are expected to facilitate opportunities in the form of flexible bioelectronics that can conform and adapt to the curved anatomy of humans (*e.g.*, health sector applications and wearable gadgets).[1-4] These materials could potentially give rise to human beings with enhanced abilities through cybernetic extensions, enable smart healthcare capable of remote and continuous patient monitoring, and maybe even ultimately change the way humans and machines interact.[3, 5]

However, most flexible electronic materials either rely on expensive and complicated metallic serpentine circuits or exotic and not that easy to scale up polymers. Ionic conductive hydrogels – an area also known as soft iononotronics – has emerged as an alternative route for developing electronic materials for human-machine-interfacing. Even though ionic conductors are less conductive than their metallic counterpart, this methodology is both more scalable and requires lesser power to run than conventional rigid electronics. In brief ionotronics operate *via* an ionic gel-like conductor that is linked to a traditional circuit operating through electron transport.[6] They are therefore also much better at mimicking the way the human body conveys information, as ion transport is one of the dominating factors in this regard. Several recent studies have capitalized upon the benefits that soft ionotronics offer to manufacture soft robots,[6] touch screens,[7-9] actuators,[10] electronic skin,[11] motion-sensors,[12-14] loud-speakers,[10] organic liquid crystal devices,[15] wearables,[12, 16] and cybernetic devices.[17] Most of these devices have been based on potentially toxic materials that are unable to heal themselves (similar to natural tissues) or adhere to them for that matter. They also display limited stretchability, quickly dehydrate to lose their functionality (> 1 h), and are unable to reconfigure properly in response to mechanical stimuli (as done by living tissues). For these reasons, they have failed to recapitulate the animated intelligence and adaptability found in natural creatures. After all, who can do it better than nature itself?

Here, we report a simple yet versatile route for creating a class of materials capable of addressing the above-mentioned shortcomings of today's ionotronics. This material has stepped up to this grand challenge by being ionic conductive, highly adhesive, reconfigurable, and viscoelastic (Care), with an almost gum-like appearance (CareGum). The

CareGum contains a limited amount of water, but not to the same extent as hydrogels. Consequently, they are not affected by the same dehydration issues that are associated with conventional hydrogels – something that usually compromise the performance of a hydrogel in dry environments. In brief, the CareGum consists of a negatively charged polymeric matrix, which has been reinforced with aligned nanotubes that form a conductive percolation network permeable for ionic transport. Notably, the CareGum can respond to external stimuli and convey it to an electronic circuit by using ionic elements. The optimized CareGum also displays electromechanical self-healing with 100% efficiency [0.5 s (electrical) and 360 s (mechanical)], is 3D printable, and can elongate up to a record high of around 30,000%; which far exceeds current records for Fe^{3+} reinforced PDMS.[18] Indeed, its shape reconfiguration ability in combination with self-healing properties is reminiscent of natural tissues, and it can, therefore, be used to yield highly advanced soft robots. As an elegant example of the power of the CareGum, we have transformed it into a wearable, electronic textile for accurate and real-time monitoring of both low and high amplitude human activities, including joint, muscle, and complicated motoric tasks. We have also attempted to add another exciting dimension to this technology by 3D printing the CareGum in a "tailor-fitted" manner on a textile sleeve to yield customizable and self-healable electronics with human-motion-sensing capacity. Generally speaking, the CareGum not only addresses a persistent challenge in materials science, but also unlocks potential applications in biomedical engineering, polymer science, electronics, and soft robotics since it exhibits many desirable properties and far outperforms the current state-of-the-art in those fields.

Results and Discussion

CareGum yields a wide range of exciting properties, including high stretchability, ionic conductivity, adhesiveness, rapid self-healing, and mechanical durability. In the following section, we performed several chemical characterizations to gain a more mechanistic understanding of this highly beneficial combination of properties. In brief, the material is composed of Polyvinyl Alcohol (PVA) (Supplementary Figure S1), Tannic Acid (TA), Ferric ions (Fe^{3+}), and polydopamine (PDA) functionalized halloysite nanotubes (HA). It is formed after a simple and scalable mixing protocol (Figure 1). The PVA component is a water-soluble polymer with many hydroxyl groups attached to its backbone, and TA is a dendritic molecule made primarily from reactive pyrogallol and catechol groups. PDA, on the other hand, presents catechol groups on its side-chains, which have been exploited by engineers

over the years to impart mussel-inspired adhesiveness and toughness onto soft materials – typically in combination with Fe^{3+}.

CareGum Characterization

From the Fourier transformation analysis (FTIR) findings in Supplementary Figure S2, it is confirmed that the hydrogen bonding between PVA and TA is the driving force behind the formation of CareGum. A detailed analysis of the data in Supplementary Figure S2a further revealed that these bonds are either strong OH-C=O between PVA and TA or weaker OH-OH between PVA-PVA and PVA-TA. Such hydrogen bonds can easily break and reform, which in theory could lead to high toughness and rapid self-healing. Another of our main hypotheses was that we could endow combinatorial properties to a soft material, such as PVA-TA (PATA), through HNT incorporation. Here, we noticed that the addition of PDA grafted HNT to PVA did not facilitate crosslinking – TA is thus solely responsible for facilitating hydrogel formation. From the FTIR analysis in Supplementary Figures S2b and S2c, it is evident that HNT incorporation shifted the peaks corresponding to C-OH (1083 cm^{-1}) and C-O-C (1024 cm^{-1}) to lower wavenumbers (1074 and 1008 cm^{-1}, respectively). We speculate that this might relate to hydrogen bonding between Si-O originating from the HNT and hydroxyl group present in the PATA composites; and thereby gives further evidence for success HNT incorporation.

We tapped into X-ray photoelectron spectroscopy (XPS) to identify the chemical interactions within the various CareGums even more (Supplementary Figure S3). As you can see in the survey spectra (Supplementary Figure S3a), the XPS signal from N 1s, Si 2p and Fe 2p confirms the existence of PDA, HNT and Fe^{3+} in the PATA-75HAF composites. The presence of C-N bond between 285-286 eV in the high-resolution spectra of carbon region (C 1s) also supported the existence of PDA in the PATA-75HA and PATA-75HAF. In addition, the decrease in C-OH (~533.0 eV) and C=O (~534.8 eV) signals in the high-resolution spectra of carbon region (O 1s) evidenced the hydrogen bond formation between PATA and HA, while the existence of Si-O (~531.3 eV) confirms the presence of HNT in the PATA-75H, PATA-75HA and PATA-75HAF composites. Furthermore, the presence of Fe-O (~530.2 eV) in the spectra for PATA-75HAF composites, is an indicator of the formation of a metal coordination complex between Fe^{3+} ions and negatively charged OH-groups between pyrogallol and catechol groups.

Interestingly, the HNTs seemed aligned even at low concentrations (Figure 2a-c); however, as the HNT concentration increased > 5%, the nanotubes began to agglomerate (Figure 2). This can potentially comprise electromechanical properties and thus needs to be addressed. Therefore, the HNTs were functionalized with PDA in an alkaline environment to yield HNT-PDA (HA); something we speculated would disperse better due to possibly more intensified interactions with PATA. The PDA coating on HNT is clearly observable as increased surface roughening in the TEM images displayed in Supplementary Figure S4b. Moreover, both the increase in zeta potential (Supplementary Figure S4c), the occurrence of N-H stretch/bend bonds in the FTIR spectra (Supplementary Figure S4d), and the increased weight loss observed from the TGA measurements (Supplementary Figure S4e) compared to pristine nanotubes are all indicators of a successful functionalization in this respect.

As predicted, PATA incorporated HA showed a high dispersion compared to pristine nanotubes, even at very high concentrations (Figures 2c and 2f). The higher dispersion might be linked with hydrogen bonds between OH groups from catechol groups in PDA and carboxylic/OH groups on PATA. Indeed, this bonding scheme enables more interactions between nanotubes and PATA and, ultimately, gives rise to core-shell like assemblies instead of nanotube-nanotube aggregations. The speculated hydrogen bonding scheme is further confirmed from the FTIR analysis (Supplementary Figure S2b and S2c). Unfortunately, the TEM image in Figure 2e shows a compromised nanotube alignment compared to the non-functionalized gums. To remedy this unwanted effect, we introduced Fe^{3+} species to further conjugate the HA with PATA (Figure 2f). This additional interaction scheme is clearly seen from the FTIR spectra in Supplementary Figure S2b and c and is in accordance with a bis metal coordination complex between Fe^{3+} ions and negatively charged OH-groups with pyrogallol and catechol groups.

Later, we used differential scanning calorimetry (DSC) to further confirm the formation of the above-mentioned intermolecular links. The pure PVA had a glass transition temperature (Tg) at around 71ºC and melting temperature (Tm) at 179ºC (Supplementary Figure S5a and S5g). As shown in Figure 2g and Table 1, the formation of PATA lowered both the Tg and Tm values of PVA. This could be due to the capacity of TA to abolish the intramolecular bonds of PVA by binding with PVA itself, as a means to inhibit its crystallization, thereby reducing its melting and glass transition point. On the contrary, the introduction of HNTs increased the Tm of the PATA composites from 126 to 140°C, something arguably caused by nucleation sites on HNT that are capable of facilitating polymer crystallization, as reported in previous studies[19]. Nevertheless, the interaction

between HNT and PATA kept the Tg-value below 60ºC (Supplementary Figure S5g). However, the incorporation of HA instead of HNT significantly increased the Tg-values of PATA composites to 63ºC at 75% HA inclusion (Supplementary Figure S5g). The increased Tg-value of the composites might be due to restricted movements of the polymer chain in the composites due to more matrix crosslinks mediated through stronger HA-PATA interactions.[20] Based on a similar rationale, the coordination bonding with Fe^{3+} ions also increases the Tg-values of the PATA, and for PATA-75HAF composites, the value reached 66ºC. The DSC observations are thus in line with the FTIR results described above.

In a similar vein, thermogravimetric analysis (TGA) was performed to study the thermal stability of the CareGums and thus the hypothesized bonding schemes in greater detail. To accurately compare the thermal stability of the composites, the temperature corresponding to a 10% weight loss ($T_{10\%}$) was selected as the reference point. All reinforced composites show enhanced thermal stability compared to that of the pristine PATA. Among all tested composites, PATA-75HAF displayed the highest thermal stability, with a $T_{10\%}$ temperature at 245°C. This is in accordance with a denser and more crosslinked matrix after HA and Fe^{3+} incorporation, since in theory more bonded materials are more difficult to thermally degrade. The TGA analysis for the remaining composites can be found in Supplementary Figure S5.

In summary, the characterization studies confirmed the presence of hierarchical bonds with varying strengths in the CareGum. The most important interactions are i) weak hydrogen bonds between PVA-PVA and catechol groups in TA/PDA; ii) stronger hydrogen bond mediated links with pyrogallol groups in TA; and iii) metal coordination bonding between Fe^{3+} and pyrogallol/catechol groups present on TA and catechol groups on PDA. The increase in the CareGum crosslinking density of PATA-75HAF compared to pristine PATA is also evident from the decrease in water content (Supplementary Figure S6) and pore size (Supplementary Figure S7).

Self-healing properties

To illustrate its self-healing capacities, the CareGum was first cut into pieces and put together to heal at room temperature (Figure 3). To distinguish the cutting site, samples were stained with red or blue dyes, and the stained gum materials were joined together to commence the healing process. Figure 3a-b shows that the healed materials are well-connected, maintain high moldability, and can sustain large strains. The interface of the cutting site reconnected rapidly (less than 360 s), and the connected parts were not damaged even after being

stretched or shaped into a circle (Figure 3b-c). To this end, we also examined the mechanical stability of the self-healed hydrogels with an Instron tensile tester. Interestingly, the destructed sections remained intact even after a large mechanical strain reaching 7450% (Figure 3c). Finally, we also employed fluorescence and scanning electron microscopy (SEM) to further highlight the self-healing capacity of the CareGum. The microscopic visualization in Figure 3d confirms a fast, dynamical restructuring of the impaired zone, which is further supported by the SEM images (Figure 3e). Overall, we can confidently state that the reversible and hierarchical bonds introduced in the previous section have performed as theorized, yielding a material with flexible reconfiguration capacity, large stretchability, and rapid self-healability.

Mechanical analysis

To further quantify the exciting properties showcased in Figure 3, we carried out a series of mechanical characterizations of the CareGums (Figure 4). Initially, all specimens were evaluated in tensile mode with an Instron mechanical tester to estimate mechanical properties, such as maximum tensile stress, Young's modulus, and strain at breakage (Figure 4a). This was done for hydrated samples, as well as for dried and re-hydrated samples (Figure 4b). Our hypothesis was that drying could facilitate the assembly of core-shell like polymeric structures around the nanotubes that remain intact after rehydration, as reported in previous studies.[21-23] In this scenario, additional crosslinks can be activated due to more intensified interactions between the soft and hard phases of the composite material. Such assemblies could potentially increase the mechanical and electrical properties.

From the stress-strain curves (Figure 4b), it is clear that re-hydrated samples display significantly larger maximum tensile stress values, with the strain at breakage remaining the same. Notably, some CareGum variants could stretch almost 30000% without breaking (Supplementary Video 1), which is many times larger than what has been reported for other materials so far.[16, 18, 24-27] In Figure 4c, the obtained stress-strain curves have been quantified to paint a more precise picture of the mechanical properties of the respective CareGums. From these quantifications, tensile strength ranging from 48 $\rightarrow$ 60 kPa and Young's modulus from 150$\rightarrow$ 166 kPa were detected for HNT reinforced PATA-xH; something that is higher than that of most hydrogels and more reminiscent of a gum-like material. The addition of ferric ions (PATA-F) resulted in a two-fold increase (48 $\rightarrow$ 75 kPa) and an almost three-fold increase (150 $\rightarrow$ 400 kPa) in tensile strength and Young's modulus, respectively. This trend

is most likely related to the formation of metal coordination bonds between TA and Fe^{+3}; since such intramolecular interactions can mitigate a denser, tougher, and much stronger polymeric network.

Likewise, the extra coordination bonds arising from HA inclusion – namely between TA and Fe^{3+} and HA and Fe^{3+} – were seen to significantly improve the mechanical properties (Figure 4c). To this end, an increase in tensile strength from 75 to 163 kPa was observed after the HA content reached 75%. Moreover, we also observed an increase in Young's modulus to around 461 kPa for HA concentrations up to 50%, and further concentration increase to 75% HA elevated the modulus even more (to 908 kPa). Oppositely, for PATA-xH, we saw a large enhancement in mechanical properties for dried and rehydrated PATA-xHAF. In brief, PATA-xH CareGums containing more than 25% HNT exhibited an almost 2-fold increase in tensile strength and Young's modulus (from 60 kPa to 100 kPa and 190 kPa to 270 kPa, respectively), without altering stretchability. For PATA with a denser network arising from the Fe^{3+} and HA incorporation (PATA-xHAF), the effect is more pronounced. The tensile strength and Young's modulus reached values of 506 kPa and 2947 kPa, respectively for PATA-75HAF - an increase that corresponds to almost 10- and 20-fold, respectively, compared to pristine PATA. These findings, supports our initial hypothesis about a drying-rehydration facilitated formation of core-shell structures – something that could result in increase surface interactions between PVA and HA and thereby greater mechanical properties. Importantly, the PDA coating enable interactions that were not possible with pristine HNT. Finally, enhanced nanotube alignment could also be a contributing factor here, in line with other reported studies.[28, 29]

We also tested the mechanical durability of CareGums for a few selected combinations: PATA-F, PATA-25HAF, and PATA-75HAF (Figure 4d). Specifically, our aim was to identify a system that could dissipate a large amount of energy without diminishing the mechanical recovery after each loading and unloading cyclic. In this direction, we exposed the selected samples to four loading/unloading cycles at 30% strain values. The energy dissipated can easily be calculated from stress-strain curves as the area bound by each cycle – the hysteresis area. For all compositions, there was a slight decrease in hysteresis between the first cycle and the subsequent cycles. After that, the hysteresis area was fairly constant. This is an indicator of a durable system capable of dissipating a substantial amount of energy, which is exactly what we were looking for. The high energy dissipation is attributed to the internal fracture of hydrogen bonds and friction occurring between adjacent nanotubes during straining. Indeed, the amount of energy dissipated relied

on the nanotube content (Figure 4d and Supplementary Figure S8) and increased almost 7-fold from 0.12 MJ/m^3 to 0.78 MJ/m^3 during the second cycle, while the nanotube concentration increased from 0% to 75%.

Furthermore, we investigated the viscoelastic (Figure 4e and f) and self-healing properties (Figure 4g and Supplementary Figure S9) of the most concentrated and durable CareGum through rheological analysis (PATA-75HAF). From the frequency sweep (Figure 4e), we observed that at frequencies above 1 rad/s, the material behaved more like a solid than a viscous liquid. Notably, both the loss and storage moduli remained in a similar range at higher frequencies, thus supporting the hypothesis that CareGum is a gum-like and viscoelastic material. These measurements also prompted us to use 10 rad/s in our downstream rheology experiments; since the value was within the viscoelastic solid range and not the liquid range. The strain-sweep measurements enabled us to determine the linear viscoelastic region (LVE) - a zone in which G' (storage modulus) and G'' (loss modulus) are almost constant, corresponding to an undisturbed material. A lot of information can be gained from this zone. For instance, if G' > G'', as shown here, the material is a viscoelastic solid. Moreover, after the modulus' decreases, the material enters a disturbed state, and when G'' > G' (crossover point), it becomes more fluid-like. Since the end of the LVE zone is 6% (Figure 4f), we can readily perform our experiments with strain values < 6% without altering the structural integrity of the tested material. On the other hand, since the crossover point is < 100%, we can expect that the material is completely destroyed for strain values of around 100%. For this reason, we decided to use 0.1% (undisturbed) and 100% (completely disturbed) to probe the cyclic healing capacity of our materials (Figure 4g). Overall, these results demonstrated that PATA-75HAF could recover in 300 s for up to three recovery cycles. The same was true for PATA-25HAF and PATA-50HAF (Supplementary Figure S10); however, the PATA-75HAF recovery was slightly compromised compared to the others (Supplementary Figure S10 & S11).

In summary, the results in Figure 4 support the hierarchical bonding scheme, which was briefly highlighted in the chemical characterization section. These results also show that our mussel-inspired and nanoreinforced PATA material increases in mechanical properties (such as Young's modulus and toughness) in the $10^{\wedge 2}$-fold range. Specifically, the material displayed energy dissipation behavior in an almost cyclic manner, which makes it ideal for use as a wearable biomaterial. In fact, high cyclic energy dissipation capacity is needed for wearable materials intended to be worn on active tissues, such as joints and muscles, as this mechanical property can significantly increase their durability. Finally, the rheology results in

Figure 4 further supported the rapid and consistent self-healing properties of CareGum revealed in Figure 3.

Adhesion studies

We also examined the adhesion properties of our composites on a wide range of surfaces, including brass, steel, glass, and PMMA, through lap-shear testing (Figure 5a-b). From these tests, we observed the highest adhesion strength for Brass and PMMA ranging from 12–28 kPa and 12–42 kPa as the nanotube concentration varied between 0–75%, respectively (Figure 5c-f). However, the reported values for glass and steel were appreciably lower, ranging from 7–13 kPa and 10–22 kPa respectively, within the same HA concentration range. This was larger than the observed adhesion strength of pristine PATA and PATA-xH on similar interfaces (Supplementary Figure S12c). The adhesion strength observed for pristine PATA is most like caused by the many available hydroxyl groups here that are capable of binding to oxygen groups on the metallic or carboxylic groups on PMMA *via* hydrogen bonds. The incorporation of HNT did not have any huge impact on the adhesion strength neither did the incorporation of Fe^{3+}. However, PDA-functionalized nanotubes (HA) had a major impact on both the adhesion to Brass, Steel, PMMA, but not Glass. This most likely stems from the extra OH-groups in this system due to the many catechol groups present on PDA. Notably, PMMA turned to be the one with the highest adhesion strength, ranging from 35 to 45 kPa for PATA-75HA and PATA-75HAF; something related to the fact that PMMA offers more OH groups for hydrogen bonds with cathechol groups on PDA than the inorganic surfaces. The adhesion of the proposed sensor onto dry surfaces that are either polymeric or metallic is of utmost importance in the development of prototype bioelectronics. Its adhesion onto wet biological tissues – especially skin – can also yield a number of exciting applications, where the sensor can directly be molded onto the skin to facilitate customized wearables for motion sensing. For this reason, its adhesiveness onto muscle and skin was also tested. While the adhesion to muscle was low, an adhesion in the range 5–8 kPa was observed for skin (Supplementary Figure S12a-b). A number of tissue adhesives exist on the market today. However, unfortunately, most of them display cytotoxicity.[30, 31] We, therefore, also tested the bio-friendliness of our adhesive sensor (Supplementary Figure S13) through C2C12 cell attachment studies, which ultimately showed no signs of material toxicity.

Electrical self-healing

The observed self-healing capacity in Figure 3-4 could potentially also give rise to electrical healing, wherein the conductivity returns back to normal following a damage-healing cycle. For this reason, we tested the electrical self-healing capacity of PATA-75HAF by designing a CareGum circuit connected to an LED light bulb (Figure 6a). We focused on PATA-75HAF, since it exhibits the best self-healing and mechanical properties. As expected, the LED was turned off immediately when the circuit was cut into two. After the two separate parts were brought together again, the circuit quickly healed, and the LED light intensity returned to its pre-cut configuration – all of this happened spontaneously and without any aid from external sources, such as light or chemical agents. During the same experiments, we also tried to fine-tune the electrical conductivity through the incorporation of higher HA content, while keeping the Fe^{3+} concentration constant (Figure 6b). As can be seen from Figure 6b, the ionic conductivity increased almost 3-fold as the HA concentration increased from 0% to 75%. We speculate that the electrical gains displayed in Figure 6 are correlated with the observed HA concentration facilitated increase in nanotube alignment. Notably, such nanotube alignments are highly sought out in the field of materials science but notoriously difficult to obtain and typically based on more complicated and hard to "get-by" technologies. [32-34] Finally, we estimated the self-healing time in Figure 6c. Here it is seen that the resistance increased to infinity when the sensor was cut in two, however, the resistance recovered to its base-level after the two separated pieces were placed together. This process took only 0.5 s.

Electromechanical analysis

To demonstrate that CareGum can be used as a biosensor compliant with curved and mechanically dynamic environments reminiscent of those present in the human body, we need to characterize its electromechanical properties. To this end, we encapsulated PATA-75HAF between an acrylic-based elastomeric substrate (VHB tape) and connected both ends with copper wires, as illustrated in Figure 6d. The VHB was use for two reasons. Firstly, to avoid water evaporating from the ionic conductive CareGum; something that potentially can alter the quality of electromechanical signals. Secondly, to be able to establish firm connections between the copper electrodes and CareGum sensor for ensuring reproducibility and repeatability within the test samples. Moreover, the high elastic properties of VHB tape also improved the electrical recovery of the CareGum sensors as is evident from the hysteresis free and almost linear-like load and unloading curve in S13 in contrast to the more viscoelastic cycles observed in Figure 4. We then proceeded to examine the relative

resistance (ΔR/R0), which is the ratio between the resistance change (ΔR) and the original resistance value (R0). These electrical experiments were carried out during twisting (Figure 5e), straining (Figure 6f), and bending (Figure 6g). As expected, the resistance increased as a function of the number of twists (53%), angle (27%), and strain (500%) within the range of 1–4 twists, 0–180°, and 0–600% strain, respectively. The increase as a function of twist and strain displayed a linear trend, whereas this linear trend only prevailed up to a rotation angle of 150° before saturating at ΔR/R0 ≈ 0.245.

From the ΔR/R0 *vs*. strain curve in Figure 6g, we also noticed that the slope and thereby the resistance increase as a function of strain was significantly lower for PATA-75HAF compared to PATA-F. It is also noteworthy that the (ΔR/R0) *vs*. strain relationship displayed a cyclic behavior for PATA-75HAF up to 10000 cycles, as evident from Supplementary Figure S14. These results are indicative of a more percolated and thereby more strain-resistive electrical network mediated by the alignment of conductive nanotubes within the PATA-75HAF matrix; befitting the assumptions made in the preceding sections. This hypothesis was examined in greater depth in Figure 6g by investigating the electromechanical behavior of PATA-75H and PATA-75HA up to 600% strain. Specifically, we utilized the gauge factor (GF=(ΔR/R0)/strain), something typically used to define the sensitivity of strain-gauge sensors, to test our hypothesis. In brief, the GF-value corresponds to the relative resistance change (ΔR/R0) at any given strain value. The higher the GF, the more sensitive the material is too small changes in strain. For this reason, the slope in a ΔR/R0 *vs*. strain curves is intimately linked with the GF, and we can thus get an impression of the GF-value from the curves shown in Figure 6g and Supplementary Figures S15. Using this sort of reasoning, one easily realizes that the GF-value drops in the following order at 600% strain: PATA-75H (GF = 2.6), PATA-75HA (GF = 1.8), PATA-75F (GF = 1.3), and PATA-75HAF (0.83) – and therefore the conductivity is the least sensitive to mechanical deformation for PATA-75HAF. One of the major differences between the groups encompassing PATA-F, PATA-75H, and PATA-75HA is the combination of more conductive elements (PDA and Fe^{+3}) and nanotube alignment in the latter group. The results described in this paragraph thus add additional value to the above-mentioned nanotube alignment hypothesis and the associated stabilized electrical conductivity. In this regard, we speculate that the observed resistance changes in Figure 6e-g are caused by a decrease in contact between the conductive HAF nanotubes within the matrix due to the mechanical deformation imposed on the sensor material. Nevertheless, this resistance change for PATA-

75HAF is not sufficiently high to compromise the electrical properties of the sensor during large strain values as compared to the other CareGum variants due to the hypothesized nanotube network. Indeed, as presented in Figure 6h, the PATA-75HAF CareGum variant is electromechanically robust and can deform, twist, and stretch without losing its electrical continuity. In summary, CareGum can be fine-tuned into a highly sensitive strain-gauge with sufficient electrical durability for it to remain operational within the various mechanically demanding regions in the human body.

CareGum as a sensing platform

To demonstrate the feasibility of the CareGum as a wearable strain sensor, we encapsulated PATA-75HAF into a VHB tape, as shown in Figure 6d and Figure 7a. Next, our proof-of-concept wearable sensor was mounted on the forefinger of a human hand to monitor its resistance change *versus* a joint bending angle (Figure 7a). As depicted in Figure 7b, we measured the finger motion by bending it from a relaxed state (0°) to a flexed state (90°) while simultaneously monitoring the resistance change with an impedance analyzer. Interestingly, it was possible to distinguish various types of finger movements (slow, fast, and step movements). Also, the relative resistance change instantly fell back to the original value once the forefinger was entirely unfolded (Figure 7b). Indeed, as can be seen from Figure 7b, the movement velocity (slow, fast, and step) gives rise to different rates of resistance changes. The developed wearable electronics, therefore, can be used to capture the dynamics of human motion, something useful in the field, but unfortunately hard to capture with today's conventional technologies.

Additionally, in the same figure, we have also demonstrated the cyclic measuring capabilities of the proposed motion sensor. The results are in accordance with the electromechanical analysis and confirm the durability of the CareGum sensor. Next, we turned our attention towards monitoring the cyclic motion of other body parts, such as wrist, shoulder, elbow, and knee (Figure 7.c-d). According to our expectations, the sensor not only recorded these movements with high fidelity but was also capable of detecting the movement amplitudes – with smaller amplitudes yielding lower ($\Delta R/R0$) values (Figure 7.d). Overall, the motion-sensing abilities shown in Figure 7 demonstrate that the sensor displays a broad range of exciting properties, while remaining scalable and low-cost. We envision that the sensing properties demonstrated in this section will be useful to decipher the complex motion patterns that come into play in various sports and music events, as well as real-time monitoring of those who are immobilized due to injury, surgery, or disease. Ideally, we

envision that the CareGum sensor will be able to assist with the rehabilitation of such patients in the foreseeable future.

3D printability of CareGum

In Figure 8a, we demonstrate that CareGum can readily blend in with the dynamic, soft, and curved anatomy of the human body in a moldable fashion. This shows its potential as a personalized wearable material that can be custom-fitted to its wearer. Notably, through 3D printing, a more precise and thereby patient-specific blending of the CareGum with the complex human anatomy is possible. In the remainder of this section, we will therefore focus on material extrusion 3D printing of the CareGum into well-defined geometries.

One of the key requirements for extrusion-printable materials is their ability to flow in response to shear; otherwise how can a material be extruded through a thin needle? This type of material is commonly denoted as pseudoplastic fluids, which means that they exhibit a shear-thinning property that enables them to be extruded with the appropriate mechanical stimuli. Therefore, we performed a series of rheological measurements to evaluate the printability of the CareGum. Here, we focused on PATA-75HAF and evaluated it at 60°C (close to its glass transition temperature) in frequency sweep mode to determine whether its shear-thinning or not (Figure 8b). Additionally, we also performed temperature sweep measurements to evaluate the viscoelastic behavior of PATA-75HAF with increasing temperature (Figure 8c). The specific goal here was to evaluate whether it is thermo-reversible – since the combination of extrusion force and temperature can be used to make an otherwise difficult to print material easier to print. From the results in Figure 8c, we observed a clear relationship between flowability (low viscosity) and temperature increase. Indeed, the viscosity dropped from 12×10^3 Pa·s to 2×10^3 Pa·s as the temperature was increased to 60°C. Next, we tried to determine the exact temperature marking the transformation of PATA-75HAF into a more liquid-like material by measuring the storage and loss modulus over time; since the point where they intersect corresponds to the phase transition from solid-to-liquid (Figure 8d). From the results in Figure 8d, we note that above 44°C the material transforms into a more liquid-like material. Notably, this transition was cyclic, as the material returned to its original gum-like properties when the temperature was gradually lowered back to room temperature. The CareGum is thus ideal for 3D printing; as it can turn to an extrudable material at high temperature and return back to its original mechanical properties following extrusion and cooling. The self-healing capacity of CareGum can also facilitate improved

printing by firstly enabling subsequent layer prints to better attach to the previously printed ones and secondly by enabling a smoothing of the deposited layers into homogenous prints. Indeed, for 3D printing applications, it is of particular importance that the viscosity is low enough to allow easy extrusion, while at the same time increasing sufficiently to avoid dripping, facilitate a firm adherence to previously deposited layers and supporting its own weight.

After the evaluation steps, we turned to a piston-driven extrusion printer with a printing head that could increase the temperature to 60°C to enable easy deposition of PATA-75HAF into complex electronic architectures (Figure 8e). As can be seen from Figure 8e and supplementary Video 2 and 3, the CareGum can be printed in different complex 3D shapes, such as cube, and cylinder at this temperature. As in the previous sections, we connected these more detailed circuitries with an LED light bulb (Figure 8f). The pictures show an intact circuit with the LED light on; after cutting the circuit in two halves, the LED stops glowing, and when the separated parts were gently pushed back together an autonomously self-healing process was facilitated. Indeed, after a few seconds, the circuit healed completely, and the LED started glowing again. Even though electrically self-healing circuits have been around for a while, the R&D of a sensor material that can readily transform into complex circuits, while displaying rapid electromechanical self-healing capacity, is still rather rare. Here, we have demonstrated this property; something that potentially could be used for the manufacture customized and super durable sensors to be used in various mechanically demanding environments.

3D-printed CareGum textiles with electronic properties

After demonstrating the electromechanical performance of PATA-75HAF and its printability through extrusion printing, we tried to utilize these properties to yield a 3D-printed human-motion sensor. Specifically, we made an attempt to print sensors with line, spiral and grid geometries onto textiles to create an electronic and wearable sleeve (Supplementary Figure S16). The reasoning for manufacturing more complicated circuits *via* 3D printing was to capture as much information from the moving body parts as possible, as their motion is directed by a complicated interplay between numerous key locomotion points. In terms of sensing fidelity, we, unfortunately, did not detect any differences between line and spiral. However, with regard to the grids, the relative resistivity dropped significantly due to the conflict between electrical signal intensity and travel distance. Therefore, for the remaining

part of this section, we solely focus on 3D printed line circuits instead, like the one shown in Figure 8d. These 3D printed sensors were further investigated in cyclic mode at different strain rates (Supplementary Figure S17a-c).

Wearable human motion sensors are not only restricted to monitoring large-strain motions, such as bending of fingers and knees prevalent during rigorous physical exercises or strenuous rehabilitation processes; they can also be applied to detect motions at a much higher frequency, such as those associated with motor disorders. We tried to capture this exciting application in Figure 8h-k by placing a 3D printed CareGum-based electronic sleeve over the brachioradialis muscle to enable hand-motion sensing (Figure 8g). Specifically, we performed a series of measurements by detecting fist-clenching, thumb, hand rotation, and more complicated hand gestures – such as those involving taking a cup, drinking water from it, and placing it back on a table; movement types that are pivotal for diagnosing Parkinson's disease. The results displayed in Figure 8h-k clearly show that we can monitor such locomotion with our 3D printed, electronic sleeve, and distinguish one from the other. Specifically, we could readily differentiate two movement patterns from one another: such as taking a cup and drinking from it and placing the palm of a hand under the chin (Figure 8j). Lastly, we were also capable of determining whether a hand rotated clockwise or counter-clockwise (Figure 8k).

Despite its great promise within a wide spectrum of applications, the field of ionotronics remains in an infant stage. Especially, their potential as material interfaces between humans and machines requires extensive further developmental work. This is partly due to the fact that the human body is exposed to load-bearing and flexing forces during daily activities. These material interfaces, therefore, need to endure repeated bending, loading, stretching and quickly self-heal in case of physical damage. To this end, the marriage between soft ionic conductive materials that can conform to the complex shapes of a human combined with electromechanical self-healing is expected to significantly increase the lifetime of such devices. Ideally, they also need to adhere to human tissues as well as inorganic interfaces to directly blend in with the body or to bond strongly with traditional silicon and metal-based circuits used in the field. For these reasons, combinatorial materials that are adhesive, tough, ionic conductive, flexible, and self-healing could potentially be used for even better human-machine-interfaces. Herein, we have developed a material that displays all of these attributes; namely the CareGum.

The many exciting properties of the CareGum were based on a wide range of interactions – both chemical and physical. Together and in the presence of Fe^{3+}, these give

rise to an ionic conductive and self-healable gum-like biomaterial mainly through OH — C=O (7.4 kcal/mol) and OH — OH (4.7 kcal/mol) hydrogen bonds.[35] Even though PVA-alone hydrogels have been manufactured over the years with some of these exhibiting self-healing and high elongation properties they have mostly been made through additional chemical modifications of PVA, by using chemical cross-linkers or *via* a freeze-thawing method.[36, 37] Here, we have shown that the addition of high concentrations of TA to a PVA solution can spontaneously yield self-healing and stretchability through a simple and scalable "design-and-mixing" procedure. To make the system printable, conductive, adhesive and strain-sensitive we turned to PDA – specifically we used high-concentrations of PDA-grafted HNT to yield aligned and percolated conductive networks. Indeed; this feature was one of the important ingredients that gave rise to the material portfolio of the CareGum. In addition, TA can also form strong metal coordination bonds (17.6 kcal/mol)[38] with Fe^{3+}. Our chemical characterization results in this direction demonstrate that both PVA and TA interact with the PDA coated nanotubes through a combination of metal coordination and hydrogen bonds. Therefore, one can claim that the CareGum matrix consists of reversible crosslinks of differing strengths based on mussel-inspired chemistry. They are thus capable of reconnecting if broken and dissipate high amounts of energy. We speculate that the resultant CareGum obtained its rapid self-healing properties in combination with material toughness and stretchability from the above-mentioned plethora of reversible and hierarchical crosslinks.

Mussel-inspired hydrogels are emerging as promising self-healing and adhesive materials –and those incorporating PDA are also recognized for turning otherwise insulating hydrogels into conductive ones.[24, 39, 40] For instance, Liu and co-workers developed mussel-inspired polyacrylamide hydrogels based on a conductive ferrofluid and carbon nanotubes (CNTs). Additionally, they also included polydopamine in this system for making the system adhesive. The adhesive properties here were in the range 13-28 kPa and thus comparable to values reported for CareGum herein; however this system was not self-healing and displayed a lower stretchability and tensile strength compared to CareGum.[39] Likewise in another recent study PEDOT was mixed with PDA-functionalized graphene oxide to yield an adhesive hydrogel with an adhesive strength in the range 20-45 kPa. Even though the adhesiveness and conductivity was substantial in this system it still suffered from low mechanical properties and did not exhibit self-healing properties.[40] In another study Han and co-workers used PDA together with nanoclay and polyacrylamide to develop an adhesive

hydrogel offering a much higher adhesiveness (28-120 kPa) than CareGum; albeit with a lower stretchability, tensile strength and lack of electromechanical response.[24] Even though CareGum taps into mussel-inspired chemistry *via* PDA it is still substantially different from what is out there at moment – primarily because of its vast material property portfolio. Indeed, it's not only adhesive and self-healing but also a 3D-printable hydrogel with high mechanical durability and great sensitivity. This in our opinion makes the major divergence between previously proposed systems and the governing reason behind the attractiveness of Caregum as a sensor material.

Moreover, TEM images (Figure 2) indicated that the conductive HA nanotubes were forming well-connected percolations networks within the CareGum matrix in an aligned manner to yield significant mechanical (20-fold) and electrical reinforcement (3-fold) (Figure 4). Importantly, from Figure 5, it was also observed that the conductivity increases by incorporating a higher amount of HA with the Fe^{3+} concentration being kept constant. Indeed, the untreated HNT particles are insulators in nature, and PDA alone is insufficient for providing an efficient conductor. Instead, the observed electrical enhancements are likely related to Fe^{3+} nanotube doping. In this scenario, the nanotube-based percolation network – which intensifies as a function of HNT concentration – can act as an electrically active tunnel-system capable of transporting ionic current. In a similar vein, our results show that the nanoreinforcement was capable of enhancing the energy dissipation capacity by almost 7-fold. We believe this to be intimately linked with the frictional forces between nanotubes that slide over one another during stretching, as reported in other related studies.[41-43] Soft materials with such high-energy dissipation capacity and tunable Young's modulus are required to enable them to perfectly meld with the many load-bearing, tough, and dissipative tissues in the body.

We also demonstrated electromechanical properties of the CareGum based on the inherent conflict between material deformation and conductivity. This intimate link has been used to develop strain-resistance sensitive sensors for monitoring various types of motions and pressure-related events. On the down side, this phenomenon can compromise electrical conductivity during flexing and bending and is thus, in some cases, a "no-go" in flexible electronics. In a worst-case scenario, during extreme straining scenarios, the resistance can also reach infinity because of electrical failure in the system. Sensors that display sufficient strain-gauge sensitivity, while enabling a fully operational sensor during flexed configurations and offering the promise of electrical healing are, therefore, not only difficult to come by, but also highly desired in the field of wearable electronics. Here we demonstrate

that our mussel-inspired and nanoreinforced ionotronic sensor covers all of these bases. Specifically, our results demonstrate that the resistance only increased by 500% after PATA-75HAF was elongated up to 600%; something lower than what is typically reported in the literature (600–1600% for 600% strain).[43-46] Additionally, traditional strain-gauge sensors based on ionic gel conductors exhibit a non-linear sensitivity to strain, which in turn significantly limits their sensing range.[26, 47-49] The PATA-75HAF CareGum variant, on the other hand, gave rise to a linear profile with an almost constant gauge-factor that only slightly changed from 0% to 600% strain. We speculate that these exciting electrical attributes of the CareGum stem from the hypothesized nanotube percolation network and denser polymeric matrix at the highest HAF concentration. This, taken together, increases the volume for ionic transport of primarily H^+, PO_4^{3-} from the buffer, but also plausibly Fe^{3+} ions, to yield a high conductivity even during extreme stretching scenarios, such as the ones displayed in Figure 5g. Finally, although the GF-value is lower here than what has been reported for conventional metal-based strain sensors (GF between 2 to 5), the poor stretchability, nonlinearity, and the lack of self-healing restrict the applications of many of these sensors under rigorous mechanical deformations.[34, 50, 51]

Even though carbon nanotubes, graphene, and metal nanowires have been used to yield electrically and mechanically self-healable materials similar to CareGum, their healing efficiency and the time required for them to heal properly are sub-optimal. Notably, after healing, many of these cannot stretch to the same extent as in their virgin states.[33, 52-54] The CareGum, on the other hand, is capable of fully reconfiguring itself at a much smaller time-scale and, thus, displays superior healing powers compared to its conventional counterparts. Moreover, several toxic responses are currently limiting the use of CNT and graphene in the field.[55-57] As an alternative, we have demonstrated that PDA functionalized HNT (HA) can yield an alternative electromechanical nanoreinforcer. Indeed, in contrast to carbon-based two-dimensional (2D) nanomaterials, HNT is made from minerals that already exist in the human body and multiple studies have shown that clay-based materials show good biocompatibility and can readily be used within the human body.[32, 58-60]

Various human-motion sensing systems have been proposed over the years, ranging from sophisticated capture imaging setups to wearable electronics based on gyroscopes, accelerometers, and magnetometers.[61-63] The latter is at the forefront of the field; however, unfortunately, they are limited by several drawbacks, such as rigidity issues, high-cost, low-sensitivity, and non-durability.[62, 64] Strain-gauge sensors could potentially address such shortcomings in the field, but few of them encompass the large portfolio of properties needed

to properly blend in with the human body, while simultaneously giving rise to high sensing fidelity. As demonstrated in the previous sections, the soft and flexible material introduced here could potentially address the "current-lack-of-methodologies" in the field and be utilized for monitoring the motion of the wrist, knee, finger, shoulder, and elbow. However, despite the burgeoning interest in using wearable electronics for healthcare monitoring, their promise within this sector has not yet been fully unleashed. One of the hitherto hidden potentials of this methodology is their customization into personalized wearable systems. In this respect, the combination of 3D scanning technology and additive manufacturing can facilitate patient-specific electronics that can custom-blend with the human body to capture as much motion-related information as possible from key locomotion points in the target tissue. Indeed, we have shown that CareGum can be 3D printed in a customizable manner on arm sleeves. We used this intelligent sleeve to capture vital motion-related information from the brachioradialis – a muscle that governs the movements of the hand. Our results demonstrate that the wearable sleeve could be used for monitoring complex hand motions, a motor movement that is typically influenced by Parkinson's disease, Alzheimer's disease, and Multiple sclerosis. Here, the patient is diagnosed by being asked to perform various hand motions, where the doctor grades the quality of these movements subjectively to give him/her a proper diagnosis (Figure 9). The 3D printed intelligent sleeve developed herein on the other hand can explore complicated hand-related motoric skills of patients objectively and continuously, and can thus give rise to a transition from subjective to objective disease diagnosis and therapy.

Conclusion

Combinatorial and soft materials with electronic properties are foreseen to become a key enabler in the field of electronics, however, substantial challenges such as production cost, scalability and compatibility with current manufacturing pipelines in the industry remains a big challenge that needs to be overcome before we can see their full potential unleashed for public view. In this study, we have attempted to address these challenges by using readily available materials in combination with non-toxic and scalable chemistry. Indeed, the manufacturing price of CareGum is 140 USD/kg (< 3000 sensors); which makes it easier to prepare for mass production, unlike many of its current rivals in the field. Notably, the facileness of the proposed methodology presented here could give rise to customizable and 3D-printed wearables covering several centimeters – all accomplished in a time-efficient and cost-effective manner. Finally, these wearables were employed for human-motion-sensing of

a wide range of motions; while displaying electromechanical durability and self-healing ability, something that will undoubtedly come handy in the mechanically demanding and highly dynamic milieus of the human body.

Methods

Preparation of modified halloysite nanotubes (HA)

The formation of halloysite-polydopamine (HA) hybrid was initiated by dissolving 1g of dopamine hydrochloride (Sigma-Aldrich, Germany) in 250 ml of Milli-Q water, followed by addition of 1g of halloysite nanotubes (HNT, Applied Minerals Inc, Sigma-Aldrich, USA). The suspension was stirred for 30 minutes to prevent HNT agglomeration. The pH value of the suspension was adjusted to pH 8.5 by Trizma® base (≥99.9%, Sigma-Aldrich, USA) and continuously stirred for 24 h at 30 ºC. The resulting black suspension was centrifuged and washed 3 times with Milli-Q water and dried at 60 ºC.

Preparation of Fe^{3+} incorporated PATA composites

Initially, stock solutions of 50 % w/v tannic acid (TA, Sigma-Aldrich, Germany), 12 % w/v of poly(vinyl alcohol) (PVA filament 1.75/0.5kg, Felix printers, Mw = 49.000, partially hydrolysed) were prepared in a phosphate buffer solution (PBS, Dulbecco's Phosphate Buffered Saline, Sigma-Aldrich, UK), while 0.1 M of iron chloride hexahydrate ($FeCl_3 \cdot 6H_2O$, Sigma Aldrich, Germany) was prepared in Milli-Q water. PVA filament was dissolved in PBS solution by stirring at 80 ˚C for 5 h until a clear PVA solution was obtained. From stock solutions 2 ml of TA solution and 2 ml of $FeCl_3 \cdot 6H_2O$ were mixed together and diluted with 10 ml of PBS. The suspension immediately turned dark green, indicating the formation of mono coordination complex with Fe^{3+}. After 15 minutes of stirring, the required amount of HA hybrid nanocomposite was gradually added under constant stirring (x = 5, 25, 50 and 75% in accordance to weight of the PVA). The mixture was continuously stirred for 24 h in order to prevent agglomeration and enhance the dispersibility of HA, while the colour of the solution began to change to dark-blue suggesting the formation of a bi-coordination complex with Fe^{3+}. Finally, 10 ml of 12% PVA solution was added and mixed with spatula until PATA-xHAF formation was fully commenced. A control sample (PATA-F) without addition of HA was also prepared using the same procedure. The prepared material was finally washed and kept for 24 hours in Milli-Q water prior to analysis.

Preparation of PATA-xH and PATA-xHA

Required amount of HA was added into 2 ml of Milli-Q water. After 15 minutes of mixing, 10 ml of 12% PVA solution was added and the solution was kept stirring for 24 hours. Finally, 2 ml of 50 % w/v TA solution was gradually added to a stirring solution and mixed with spatula until the formation of PATA-xHA was completed. A sample with unmodified HNT (PATA-xH) was prepared following the same protocol, while PATA was obtained by adding 2 ml of TA solution directly into 10 ml of PVA. The prepared CareGum was finally washed and kept for 24 hours in Milli-Q water prior to the analysis.

CareGum Characterization

Gel permeation chromatography (GPC): was carried out to determine the average molecular weight (Mw) and the number average molecular weight (Mn) of PVA filament. To this end, PVA filament was dried in an oven at 60 oC for 4 hours and dissolved in water at 80°C in order to prepare 2.5 mg/mL solution. Shimadzu RID-10A detector in series with Viscotek, Dual Light Scattering detector, TriSec Model 270 was utilized, along with a set of TSK PW-type columns of pore sizes 4000 and 2500. The mobile phase was acetonitrile-water (20:80)/0.05 sodium nitrate. The GPC flow rate was adjusted to 0.5 ml/min at a temperature of 40 ºC, while the injection volume was 0.2 mL. LS-detector constants were calibrated with Poly(ethylene oxide). Data were analysed with Viscotek TriSEC GPC Software.

Proton Nuclear Magnetic Resonance (^{1}H NMR) Characterization: PVA filament was dissolved in D_2O (10 mg/mL) and placed in NMR tubes. The chemical composition was confirmed by a Varian Mercury 400 MHz spectrometer.

Zeta potential: was evaluated to determine the effect of polydopamine on the surface charge of halloysite by using a Malvern Zetasizer ZS apparatus (UK) equipped with a 4 mW HeNe laser that was operated at 632.8 nm. The measurements were performed at four different pH values at 25 °C for dilute HNT and HA suspensions (0.25 mg/mL) in Milli-Q water. The pH was adjusted using 0.1 M HCl and 0.1 M NaOH. Zeta potential values were reported as the average of three independent measurements and three measurements were performed on each sample.

X-ray photoelectron spectroscopy (XPS): of the freeze-dried PATA composites were carried out using XPS K-Alpha from Thermo Scientific with a monochromated Al Kα X-ray source with a photon energy of 1486.6 eV and ultrahigh vacuum (~10-8 mbar). All spectra were analysed and deconvoluted using Thermo Avantage v5.988 (Thermo Fischer Scientific, UK).

Thermogravimetric analysis (TGA): was carried out with TGA Q500 Thermogravimetric analyzer (TA Instruments, USA) from 30 to 900 °C with a rate of 10 °C/min. The mass loss of dried and ground hydrogels was monitored as function of temperature, under a constant nitrogen flow at 60 mL/min.

Differential Scanning Calorimetry (DSC): was performed with DSC Q200 (TA Instruments). In brief, dried and ground hydrogels (5-10 mg) were placed in Tzero aluminium pans (Switzerland) and sealed. The measurements were performed between 25 to 300 °C using an increase of 10 °C/min, under a nitrogen flow of 50 mL/min. The heat flow change is measured as a function of temperature with reference to an empty pan.

Scanning Electron Microscopy (SEM): observations were performed by FEI Quanta 200 ESEM FEG equipped with a field emission gun (Thermo Fisher Scientific, Waltham, USA). The observations were carried out on cross-sectional images of hydrogels with acceleration voltage of 3 kV. Samples for SEM observations were formed in a thin cylindrical shape and swelled in water for 24 h. Afterwards, samples were freeze-dried and cut in order to image the inner side of the hydrogel. All samples were coated with 10 nm gold layer by Quorum coater Q150T (Quorum Technologies, UK) prior to imaging.

Transmission Electron Microscopy (TEM): observations were performed by FEI Tecnai T20 G2 (Thermo Fisher Scientific, Waltham, USA) operating at 200 kV located at the Center for Electron Nanoscopy at DTU. Images were acquired using a CCD camera equipped with Digital Micrograph (Gatan, Pleasanton, USA). A 3 µL suspension of HNT and HA was drop casted onto freshly glow discharged 400 mesh copper TEM grids (Ted Pella, Redding, USA) and allowed to adsorb for 5 minutes before the excess liquid was removed with filter paper. In order to observe the alignment of HNT nanotubes within PATA, small pieces of composite material, less than 1 x 1 mm in cross section were placed in silicon molds (Pelco 10590, Ted Pella, Redding, USA) and oriented such that the HNT nanotubes were perpendicular to the mold face. The molds were then filled with Agar 100 epoxy resin (Agar Scientific, Standsted, UK) and placed in a 60 °C oven overnight to cure. After curing, the resin-embedded samples were trimmed using a razor blade ensuring that the composite on the block face was entirely encompassed in resin, to minimize uneven swelling of the composite. Thin sections of ~250 nm were then cut using a RMC MT-7 ultramicrotome (Boeckeler Instruments, Tucson, USA) and placed on 200 mesh nickel TEM grids coated with a carbon stabilized formvar film (Electron Microscopy Sciences, Hatfield, USA).

Water content: was determined by measuring the weight of the freeze-dried (W_d) hydrogels after swelling in Milli-Q water for 24 hours (W_w). The water content (%) was calculated using the following equation:

$$\text{Water content (\%)} = \frac{W_w - W_d}{W_w} \cdot 100\%$$

Mechanical tensile testing: was performed on a universal test machine Instron 5967 with 500 N load cell. Samples were molded and cut into a rectangular shape of 14 mm in width, 22 mm in length and 1 mm in thickness. The gauge length was set to 2 mm. The samples were pulled apart at a speed of 100 mm/min until failure occurred. All samples were kept in MilliQ-water for 24 hours prior to the measurement. The samples were also subjected to mechanical studies after drying at room temperature and rehydrating in Milli-Q water for 18 h. These samples were named reswelled samples. The samples were also subjected to cyclic stretching measurements at a speed of 10 mm/min.

Adhesion tests: were performed on a universal test machine Instron 5967 with 500 N load cell to investigate the shear adhesive strength of the hydrogels. Measurements were performed using glass, steel and brass at room temperature under wet conditions. Specimens were prepared measuring 12.7 mm x 25.4 mm and placed in between the substrates. Subsequently and prior to the tests a 100 g weight was applied on the prepared setup for 1 hour. The tests were performed also on animal tissues: porcine skin and muscles procured from the local slaughterhouse. The tissues were cut into 10 mm x 40 mm pieces with thickness of ~5 mm, while the sample dimensions were 10 mm x 10 mm. 6 specimens were arranged in between two pieces of fresh tissues and placed in 37 °C PBS with applied 100 g weight for 10 minutes. Shear tensile measurements were performed at a speed of 10 mm/min.

Rheology: The viscoelastic behaviour of CareGums was characterized by Discovery Hybrid Rheometer HR-2, TA Instruments with parallel plates each measuring 20 mm in diamter. All samples were measured at a gap size of 1 mm. The linear-viscoelastic region (LVE) was evaluated from an amplitude sweep, performed from 0.1 to 100% at a fixed angular frequency of 10 rad/s and the angular frequency sweep test were performed from 0.01 to 150 rad/s at a constant 0.1% strain. Finally, the self-healing ability of hydrogels was evaluated under strain step measurement, switching from 0.1% to 100% strain (angular frequency 10 rad/s) with 300 s for every interval and with a recovery time of 360 s.

Ionic conductivity: Electrochemical Impedance Spectroscopy (EIS) was performed in order to evaluate the ionic conductivity of the hydrogels. Measurements were performed utilizing Gamry Potentiostat (USA), where a 10 mV ac voltage was swept from 100 kHz to 10 Hz. CareGum samples were then prepared in a size of 1 cm^2, and were sandwiched between two stainless steel plates. The plates were connected to the impedance analyzer and Nyquist data were collected using Gamry Instruments Framework software. The Nyquist curve was fitted using EC-Lab software (Bio-Logic Science instruments) to determine the solution resistance (R_s) and ionic conductivity (σ) was calculated according to the following equation:

$$\sigma = \frac{1}{R_s} \cdot \frac{l}{a}$$

where l and a are the thickness of the sample and sandwiched area, respectively.

Resistance measurements: Resistance measurements during stretching were performed with an Agilent 4294A precision impedance analyzer (USA). For stretching, samples measuring 1 cm x 3 cm x 0.1 cm were molded and two copper electrodes were attached to each end. The samples were sandwiched between two 1 mm thick VHB (4910, 3M) tape. The stretching of the samples was performed by a custom-build linear actuator exhibiting a controlled strain rate. The distance between the electrodes was 1 cm, while the samples were pulled apart at a speed of 25 mm/min. The resistance and strain rate were recorded using a custom-made software interface. The analyser was set to measure impedance amplitude *versus* time. All measurements were performed at a fixed frequency of 2 kHz with an ac excitation voltage of 0.5 V amplitude. The power usage for motion sensing was therefore low and within the safe range for humans. Relative resistance ($\Delta R/R_0$) was then calculated from the measured values. The resistance change on the cyclic stretching was monitored at different strain rates such as 50, 100, 150, 200 and 600%. Moreover, twisting and bending measurements were performed on a sample where the distance between the electrode was 3 cm. The resistance change of the sample was recorded during manual twisting or different bending angles using a custom-build platform.

Human Motion Sensing: For motion sensing sensors with different distance between them and the copper electrodes (3 and 6.5 cm) were encapsulated in VHB tape (4910, 3M) as described previously. Sensors were made 3 cm long for monitoring the motion of finger and wrist, while the sensors used for monitoring the motion of knee, elbow and shoulder were

measuring 6.5 cm. Real-time monitoring of relative resistances with response to body movements was monitored using Agilent 4294A precision impedance analyzer (USA).

CareGum 3D printing: The samples were extruded onto stretchable fabric using a desktop 3D printer equipped with a heated syringe instead of a conventional filament extruder (Engine SR, Hyrel3D, USA). The extrusion nozzle had a diameter of 1.5 mm, and the syringe was kept at 60 °C during the material deposition. The motion of the printing head was prescribed using G-code that specifies the position of the extrusion orifice in Cartesian coordinates at various time-points. The velocity of the printing head motion was 2.5 mm/s, and the layer height was set to 2.5 mm. The speed of the stepper motor driving the syringe piston was adjusted to achieve a smooth outflow of material from the orifice.

For the strain sensing, the printed structure was encapsulated in VHB (4910, 3M) and stretching measurements were performed as described previously. Additionally, the signals from the muscle were evaluated with different physical activity of the hand. Ethical permission was obtained from local authorities and informed signed consent was obtained from all study participants involved in the research.

CareGum cytotoxicity: Murine C2C12 myoblasts cells (passage nr 16) were cultured in DMEM supplemented with FBS 10% (v/v), penicillin–streptomycin (1% v/v) and incubated at 37 °C and 5% CO_2. Cells were detached from flasks at 70% confluency by trypsinization; and they were either sub-cultured or used for the experiments. To evaluate the cytotoxicity of C2C12 cells, 1×106 cells per ml cells suspension was added into the 6 well culture plates (2 ml) and left over night to enable the cells to attach and spread. Furthermore, 4 ml of C2C12 growth media was added to each well and 100 mg of the sample was placed in an insert body and immersed into culture wells. The samples were incubated for 24 hours and evaluated with light microscopy with different magnifications to observe the cells and evaluate their well-being.

Supporting Information

The Supporting Information is available free of charge at http://pubs.acs.org

Chemical analysis of PVA, FTIR analysis of CareGums, XPS analysis of PATA composites, Modification of halloysite nanotubes (HNT) with polydopamine (PDA), Thermal analysis of CareGums, Determination of water content, SEM images presenting the pore size of CareGums, Cycle stretching measurements, Healing efficiency of mechanical performance

for PATA-75HAF CareGums, Rheology of of CareGums containing 25 and 50 % nanotubes, SEM images showing PATA-75HAF self-healing, Adhesive properties on tissues, CareGum cytotoxicity, Electromechanical supplementary studies, Photographs presenting 3D printed CareGum patterns on stretchable fabrics, CareGum printability.

Acknowledgements

ADP would like to acknowledge the Danish Council for Independent Research (Technology and Production Sciences, 8105–00003B), the Villum Foundation (10103) and the VIDI research programme with project number R0004387, which is (partly) financed by the Netherlands Organisation for Scientific Research (NWO). MPS and JS were supported by the Danish Council for Independent Research (DFF) | Technology and Production Sciences (FTP) (Contract No. 7017-00128).

References:

1. Liao, C. Z.; Zhang, M.; Yao, M. Y.; Hua, T.; Li, L.; Yan, F., Flexible Organic Electronics in Biology: Materials and Devices. *Adv. Mater.* **2015,** *27* (46), 7493-7527.

2. Kim, D. H.; Viventi, J.; Amsden, J. J.; Xiao, J. L.; Vigeland, L.; Kim, Y. S.; Blanco, J. A.; Panilaitis, B.; Frechette, E. S.; Contreras, D.; Kaplan, D. L.; Omenetto, F. G.; Huang, Y. G.; Hwang, K. C.; Zakin, M. R.; Litt, B.; Rogers, J. A., Dissolvable Films of Silk Fibroin for Ultrathin Conformal Bio-Integrated Electronics. *Nat. Mater.* **2010,** *9* (6), 511-517.

3. Lim, H. R.; Kim, H. S.; Qazi, R.; Kwon, Y. T.; Jeong, J. W.; Yeo, W. H., Advanced Soft Materials, Sensor Integrations, and Applications of Wearable Flexible Hybrid Electronics in Healthcare, Energy, and Environment. *Adv. Mater.* **2020,** *32* (15), 1901924.

4. Choi, S.; Han, S. I.; Jung, D.; Hwang, H. J.; Lim, C.; Bae, S.; Park, O. K.; Tschabrunn, C. M.; Lee, M.; Bae, S. Y.; Yu, J. W.; Ryu, J. H.; Lee, S. W.; Park, K.; Kang, P. M.; Lee, W. B.; Nezafat, R.; Hyeon, T.; Kim, D. H., Highly Conductive, Stretchable and Biocompatible Ag-Au Core-Sheath Nanowire Composite for Wearable and Implantable Bioelectronics. *Nat. Nanotechnol.* **2018,** *13* (11), 1048-1056.

5. Mehrali, M.; Bagherifard, S.; Akbari, M.; Thakur, A.; Mirani, B.; Mehrali, M.; Hasany, M.; Orive, G.; Das, P.; Emneus, J.; Andresen, T. L.; Dolatshahi-Pirouz, A., Blending Electronics with the Human Body: A Pathway toward a Cybernetic Future. *Adv. Sci.* **2018,** *5* (10), 1700931.

6. Yang, C. H.; Suo, Z. G., Hydrogel Ionotronics. *Nat. Rev. Mater.* **2018,** *3* (6), 125-142.

7. Kadumudi, F. B.; Jahanshahi, M.; Mehrali, M.; Zsurzsan, T. G.; Taebnia, N.; Hasany, M.; Mohanty, S.; Knott, A.; Godau, B.; Akbari, M.; Dolatshahi-Pirouz, A., A Protein-Based, Water-Insoluble, and Bendable Polymer with Ionic Conductivity: A Roadmap for Flexible and Green Electronics. *Adv. Sci.* **2019,** *6* (5), 1801241.

8. Kim, C. C.; Lee, H. H.; Oh, K. H.; Sun, J. Y., Highly Stretchable, Transparent Ionic Touch Panel. *Science* **2016,** *353* (6300), 682-687.

9. Sarwar, M. S.; Dobashi, Y.; Preston, C.; Wyss, J. K. M.; Mirabbasi, S.; Madden, J. D. W., Bend, Stretch, and Touch: Locating a Finger on an Actively Deformed Transparent Sensor Array. *Sci. Adv.* **2017,** *3* (3), e1602200.

10. Keplinger, C.; Sun, J. Y.; Foo, C. C.; Rothemund, P.; Whitesides, G. M.; Suo, Z. G., Stretchable, Transparent, Ionic Conductors. *Science* **2013,** *341* (6149), 984-987.

11. Larson, C.; Peele, B.; Li, S.; Robinson, S.; Totaro, M.; Beccai, L.; Mazzolai, B.; Shepherd, R., Highly Stretchable Electroluminescent Skin for Optical Signaling and Tactile Sensing. *Science* **2016,** *351* (6277), 1071-1074.

12. Lei, Z. Y.; Wang, Q. K.; Sun, S. T.; Zhu, W. C.; Wu, P. Y., A Bioinspired Mineral Hydrogel as a Self-Healable, Mechanically Adaptable Ionic Skin for Highly Sensitive Pressure Sensing. *Adv. Mater.* **2017,** *29* (22), 1700321.

13. Gao, Y.; Jia, F.; Gao, G. H., Transparent and Conductive Amino Acid-Tackified Hydrogels as Wearable Strain Sensors. *Chem. Eng. J.* **2019,** *375,* 121915.

14. Guan, L.; Yan, S.; Liu, X.; Li, X. Y.; Gao, G. H., Wearable Strain Sensors Based on Casein-Driven Tough, Adhesive and Anti-Freezing Hydrogels for Monitoring Human-Motion. *J. Mat. Chem. B* **2019,** *7* (34), 5230-5236.

15. Yang, C. H.; Zhou, S.; Shian, S.; Clarke, D. R.; Suo, Z. G., Organic Liquid-Crystal Devices Based on Ionic Conductors. *Mater. Horizons* **2017,** *4* (6), 1102-1109.

16. Pu, X.; Liu, M. M.; Chen, X. Y.; Sun, J. M.; Du, C. H.; Zhang, Y.; Zhai, J. Y.; Hu, W. G.; Wang, Z. L., Ultrastretchable, Transparent Triboelectric Nanogenerator as Electronic Skin for Biomechanical Energy Harvesting and Tactile Sensing. *Sci. Adv.* **2017,** *3* (5), e1700015.

17. Wan, C.; Xiao, K.; Angelin, A.; Antonietti, M.; Chen, X., The Rise of Bioinspired Ionotronics. *Advanced Intelligent Systems* **2019,** *1* (7), 1900073.

18. Li, C. H.; Wang, C.; Keplinger, C.; Zuo, J. L.; Jin, L.; Sun, Y.; Zheng, P.; Cao, Y.; Lissel, F.; Linder, C.; You, X. Z.; Bao, Z. A., A Highly Stretchable Autonomous Self-Healing Elastomer. *Nat. Chem.* **2016,** *8* (6), 619-625.

19. Liu, M.; Guo, B.; Du, M.; Jia, D., Drying Induced Aggregation of Halloysite Nanotubes in Polyvinyl Alcohol/Halloysite Nanotubes Solution and Its Effect on Properties of Composite Film. *Applied Physics A* **2007,** *88* (2), 391-395.

20. Xiong, S.; Wang, Y.; Yu, J.; Chen, L.; Zhu, J.; Hu, Z., Polydopamine Particles for Next-Generation Multifunctional Biocomposites. *Journal of Materials Chemistry A* **2014,** *2* (20), 7578-7587.

21. Wang, J. F.; Lin, L.; Cheng, Q. F.; Jiang, L., A Strong Bio-Inspired Layered PNIPAM-Clay Nanocomposite Hydrogel. *Angew. Chem.-Int. Edit.* **2012,** *51* (19), 4676-4680.

22. Podsiadlo, P.; Kaushik, A. K.; Arruda, E. M.; Waas, A. M.; Shim, B. S.; Xu, J. D.; Nandivada, H.; Pumplin, B. G.; Lahann, J.; Ramamoorthy, A.; Kotov, N. A., Ultrastrong And Stiff Layered Polymer Nanocomposites. *Science* **2007,** *318* (5847), 80-83.

23. Morits, M.; Verho, T.; Sorvari, J.; Liljestrom, V.; Kostiainen, M. A.; Groschel, A. H.; Ikkala, O., Toughness and Fracture Properties in Nacre-Mimetic Clay/Polymer Nanocomposites. *Adv. Funct. Mater.* **2017,** *27* (10), 1605378.

24. Han, L.; Lu, X.; Liu, K. Z.; Wang, K. F.; Fang, L. M.; Weng, L. T.; Zhang, H. P.; Tang, Y. H.; Ren, F. Z.; Zhao, C. C.; Sun, G. X.; Liang, R.; Li, Z. J., Mussel-Inspired Adhesive and Tough Hydrogel Based on Nanoclay Confined Dopamine Polymerization. *Acs Nano* **2017,** *11* (3), 2561-2574.

25. Qiao, H. Y.; Qi, P. F.; Zhang, X. H.; Wang, L. A.; Tan, Y. Q.; Luan, Z. H.; Xia, Y. Z.; Li, Y. H.; Sui, K. Y., Multiple Weak H-Bonds Lead to Highly Sensitive, Stretchable, Self Adhesive, and Self-Healing Ionic Sensors. *ACS Appl. Mater. Interfaces* **2019,** *11* (8), 7755-7763.

26. Zhang, Y. Z.; Lee, K. H.; Anjum, D. H.; Sougrat, R.; Jiang, Q.; Kim, H.; Alshareefit, H. N., Mxenes Stretch Hydrogel Sensor Performance to New Limits. *Sci. Adv.* **2018,** *4* (6), eaat0098.

27. Han, L.; Yan, L. W.; Wang, K. F.; Fang, L. M.; Zhang, H. P.; Tang, Y. H.; Ding, Y. H.; Weng, L. T.; Xu, J. L.; Weng, J.; Liu, Y. J.; Ren, F. Z.; Lu, X., Tough, Self-Healable and Tissue-Adhesive Hydrogel with Tunable Multifunctionality. *NPG Asia Mater.* **2017,** *9*(4), e372-e372.

28. Zhao, X.; Zhou, C.; Liu, M., Self-Assembled Structures of Halloysite Nanotubes: Towards the Development of High-Performance Biomedical Materials. *J. Mat. Chem. B* **2020,** *8*(5), 838-851.

29. Zhao, N. N.; Liu, Y. L.; Zhao, X. M.; Song, H. Z., Liquid Crystal Self-Assembly Of Halloysite Nanotubes In Ionic Liquids: A Novel Soft Nanocomposite Ionogel Electrolyte with High Anisotropic Ionic Conductivity and Thermal Stability. *Nanoscale* **2016,** *8* (3), 1545-1554.

30. Pascual, G.; Sotomayor, S.; Rodriguez, M.; Perez-Kohler, B.; Kuhnhardt, A.; Fernandez-Gutierrez, M.; San Roman, J.; Bellon, J. M., Cytotoxicity of Cyanoacrylate-Based Tissue Adhesives and Short-Term Preclinical *in Vivo* Biocompatibility in Abdominal Hernia Repair. *PLoS One* **2016,** *11* (6), e0157920.

31. Bre, L. P.; Zheng, Y.; Pego, A. P.; Wang, W. X., Taking Tissue Adhesives To the Future: From Traditional Synthetic to New Biomimetic Approaches. *Biomater. Sci.* **2013,** *1* (3), 239-253.

32. Zhao, X. J.; Zhou, C. R.; Lvov, Y.; Liu, M. X., Clay Nanotubes Aligned with Shear Forces for Mesenchymal Stem Cell Patterning. *Small* **2019,** *15* (21), 1900357.

33. Zhang, R. Z.; Ding, J. J.; Liu, C.; Yang, E. H., Highly Stretchable Supercapacitors Enabled by Interwoven CNTs Partially Embedded in PDMS. *ACS Appl. Energ. Mater.* **2018,** *1* (5), 2048-2055.

34. Yamada, T.; Hayamizu, Y.; Yamamoto, Y.; Yomogida, Y.; Izadi-Najafabadi, A.; Futaba, D. N.; Hata, K., A Stretchable Carbon Nanotube Strain Sensor for Human-Motion Detection. *Nat. Nanotechnol.* **2011,** *6* (5), 296-301.

35. Steiner, T., The Hydrogen Bond in the Solid State. *Angew. Chem.-Int. Edit.* **2002,** *41* (1), 48-76.

36. Chen, Y.-N.; Peng, L.; Liu, T.; Wang, Y.; Shi, S.; Wang, H., Poly (Vinyl Alcohol)–Tannic Acid Hydrogels with Excellent Mechanical Properties and Shape Memory Behaviors. *ACS applied materials & interfaces* **2016,** *8* (40), 27199-27206.

37. Zhang, H.; Xia, H.; Zhao, Y., Poly (Vinyl Alcohol) Hydrogel Can Autonomously Self-Heal. *Acs Macro Letters* **2012,** *1* (11), 1233-1236.

38. Kazmi, S. A.; Qureshi, M. S.; Maqsood, Z., Reactivity of an Iron(III) Complex of Gallic Acid. *Inorganica Chimica Acta-Bioinorganic Chemistry* **1987,** *137* (3), 151-154.

39. Liu, K.; Han, L.; Tang, P.; Yang, K.; Gan, D.; Wang, X.; Wang, K.; Ren, F.; Fang, L.; Xu, Y., An Anisotropic Hydrogel Based on Mussel-Inspired Conductive Ferrofluid Composed of Electromagnetic Nanohybrids. *Nano Letters* **2019,** *19* (12), 8343-8356.

40. Gan, D.; Huang, Z.; Wang, X.; Jiang, L.; Wang, C.; Zhu, M.; Ren, F.; Fang, L.; Wang, K.; Xie, C., Graphene Oxide-Templated Conductive and Redox-Active Nanosheets Incorporated Hydrogels for Adhesive Bioelectronics. *Advanced Functional Materials* **2020,** *30* (5), 1907678.

41. Du, R.; Wu, J. X.; Chen, L.; Huang, H.; Zhang, X. T.; Zhang, J., Hierarchical Hydrogen Bonds Directed Multi-Functional Carbon Nanotube-Based Supramolecular Hydrogels. *Small* **2014,** *10* (7), 1387-1393.

42. Dai, S. P.; Zhou, X. S.; Wang, S.; Ding, J. N.; Yuan, N. Y., A Self-Healing Conductive and Stretchable Aligned Carbon Nanotube/Hydrogel Composite with a Sandwich Structure. *Nanoscale* **2018,** *10* (41), 19360-19366.

43. Cai, G. F.; Wang, J. X.; Qian, K.; Chen, J. W.; Li, S. H.; Lee, P. S., Extremely Stretchable Strain Sensors Based on Conductive Self-Healing Dynamic Cross-Links Hydrogels for Human-Motion Detection. *Adv. Sci.* **2017,** *4* (2), 1600190.

44. Sun, X.; Qin, Z.; Ye, L.; Zhang, H.; Yu, Q.; Wu, X.; Li, J.; Yao, F., Carbon Nanotubes Reinforced Hydrogel as Flexible Strain Sensor with High Stretchability and Mechanically Toughness. *Chem. Eng. J.* **2020,** *382,* 122832.

45. Chen, J. S.; Peng, Q. Y.; Thundat, T.; Zeng, H. B., Stretchable, Injectable, and Self-Healing Conductive Hydrogel Enabled by Multiple Hydrogen Bonding toward Wearable Electronics. *Chem. Mat.* **2019,** *31* (12), 4553-4563.

46. Yang, B. W.; Yuan, W., Highly Stretchable and Transparent Double-Network Hydrogel Ionic Conductors as Flexible Thermal-Mechanical Dual Sensors and Electroluminescent Devices. *ACS Appl. Mater. Interfaces* **2019,** *11* (18), 16765-16775.

47. Xia, S.; Song, S. X.; Jia, F.; Gao, G. H., A Flexible, Adhesive and Self-Healable Hydrogel-Based Wearable Strain Sensor for Human Motion and Physiological Signal Monitoring. *J. Mat. Chem. B* **2019,** *7* (30), 4638-4648.

48. Shao, C. Y.; Wang, M.; Meng, L.; Chang, H. L.; Wang, B.; Xu, F.; Yang, J.; Wan, P. B., Mussel-Inspired Cellulose Nanocomposite Tough Hydrogels with Synergistic Self-Healing, Adhesive, and Strain-Sensitive Properties. *Chem. Mat.* **2018,** *30* (9), 3110-3121.

49. Wang, Z. W.; Chen, J.; Wang, L. F.; Gao, G. R.; Zhou, Y.; Wang, R.; Xu, T.; Yin, J. B.; Fu, J., Flexible and Wearable Strain Sensors Based on Tough and Self-Adhesive Ion Conducting Hydrogels. *J. Mat. Chem. B* **2019,** *7* (1), 24-29.

50. Yang, S. X.; Lu, N. S., Gauge Factor and Stretchability of Silicon-on-Polymer Strain Gauges. *Sensors* **2013,** *13* (7), 8577-8594.

51. Zheng, Q. B.; Liu, X.; Xu, H. R.; Cheung, M. S.; Choi, Y. W.; Huang, H. C.; Lei, H. Y.; Shen, X.; Wang, Z. Y.; Wu, Y.; Kim, S. Y.; Kim, J. K., Sliced Graphene Foam Films for Dual-Functional Wearable Strain Sensors and Switches. *Nanoscale Horiz.* **2018,** *3* (1), 35-44.

52. Son, D.; Kang, J.; Vardoulis, O.; Kim, Y.; Matsuhisa, N.; Oh, J. Y.; To, J. W. F.; Mun, J. W.; Katsumata, T.; Liu, Y. X.; McGuire, A. F.; Krason, M.; Molina-Lopez, F.; Ham, J.; Kraft, U.; Lee, Y.; Yun, Y.; Tok, J. B. H.; Bao, Z. N., An Integrated Self-Healable Electronic Skin System Fabricated *via* Dynamic Reconstruction of a Nanostructured Conducting Network. *Nat. Nanotechnol.* **2018,** *13* (11), 1057-1065.

53. Gong, C. K.; Liang, J. J.; Hu, W.; Niu, X. F.; Ma, S. W.; Hahn, H. T.; Pei, Q. B., A Healable, Semitransparent Silver Nanowire-Polymer Composite Conductor. *Adv. Mater.* **2013,** *25* (30), 4186-4191.

54. Wang, H.; Zhu, B. W.; Jiang, W. C.; Yang, Y.; Leow, W. R.; Wang, H.; Chen, X. D., A Mechanically and Electrically Self-Healing Supercapacitor. *Adv. Mater.* **2014,** *26* (22), 3638-3643.

55. Zhang, Y. B.; Ali, S. F.; Dervishi, E.; Xu, Y.; Li, Z. R.; Casciano, D.; Biris, A. S., Cytotoxicity Effects of Graphene and Single-Wall Carbon Nanotubes in Neural Phaeochromocytoma-Derived PC12 Cells. *ACS Nano* **2010,** *4* (6), 3181-3186.

56. Yuan, X.; Zhang, X. X.; Sun, L.; Wei, Y. Q.; Wei, X. W., Cellular Toxicity and Immunological Effects of Carbon-based Nanomaterials. *Part. Fibre Toxicol.* **2019,** *16*(1), 1-27.

57. Martin, C.; Kostarelos, K.; Prato, M.; Bianco, A., Biocompatibility and Biodegradability of 2D Materials: Graphene and Beyond. *Chem. Commun.* **2019,** *55* (39), 5540-5546.

58. Gaharwar, A. K.; Cross, L. M.; Peak, C. W.; Gold, K.; Carrow, J. K.; Brokesh, A.; Singh, K. A., 2D Nanoclay for Biomedical Applications: Regenerative Medicine, Therapeutic Delivery, and Additive Manufacturing. *Adv. Mater.* **2019,** *31* (23), 1900332.

59. Santos, A. C.; Ferreira, C.; Veiga, F.; Ribeiro, A. J.; Panchal, A.; Lvov, Y.; Agarwal, A., Halloysite Clay Nanotubes for Life Sciences Applications: From Drug Encapsulation to Bioscaffold. *Adv. Colloid Interface Sci.* **2018,** *257*, 58-70.

60. Mousa, M.; Evans, N. D.; Oreffo, R. O. C.; Dawson, J. I., Clay Nanoparticles for Regenerative Medicine and Biomaterial Design: A Review of Clay Bioactivity. *Biomaterials* **2018,** *159*, 204-214.

61. Zhu, R.; Zhou, Z. Y., A Real-Time Articulated Human Motion Tracking Using Tri-Axis Inertial/Magnetic Sensors Package. *IEEE Trans. Neural Syst. Rehabil. Eng.* **2004,** *12* (2), 295-302.

62. Zhou, H. Y.; Hu, H. S., Human Motion Tracking for Rehabilitation - A Survey. *Biomed. Signal Process. Control* **2008,** *3* (1), 1-18.

63. Boonstra, M. C.; van der Slikke, R. M. A.; Keijsers, N. L. W.; van Lummel, R. C.; Malefijt, M. C. D.; Verdonschot, N., The Accuracy of Measuring the Kinematics of Rising from a Chair with Accelerometers and Gyroscopes. *J. Biomech.* **2006,** *39* (2), 354-358.

64. Servati, A.; Zou, L.; Wang, Z. J.; Ko, F.; Servati, P., Novel Flexible Wearable Sensor Materials and Signal Processing for Vital Sign and Human Activity Monitoring. *Sensors* **2017,** *17* (7), 1622.

Figures and captions

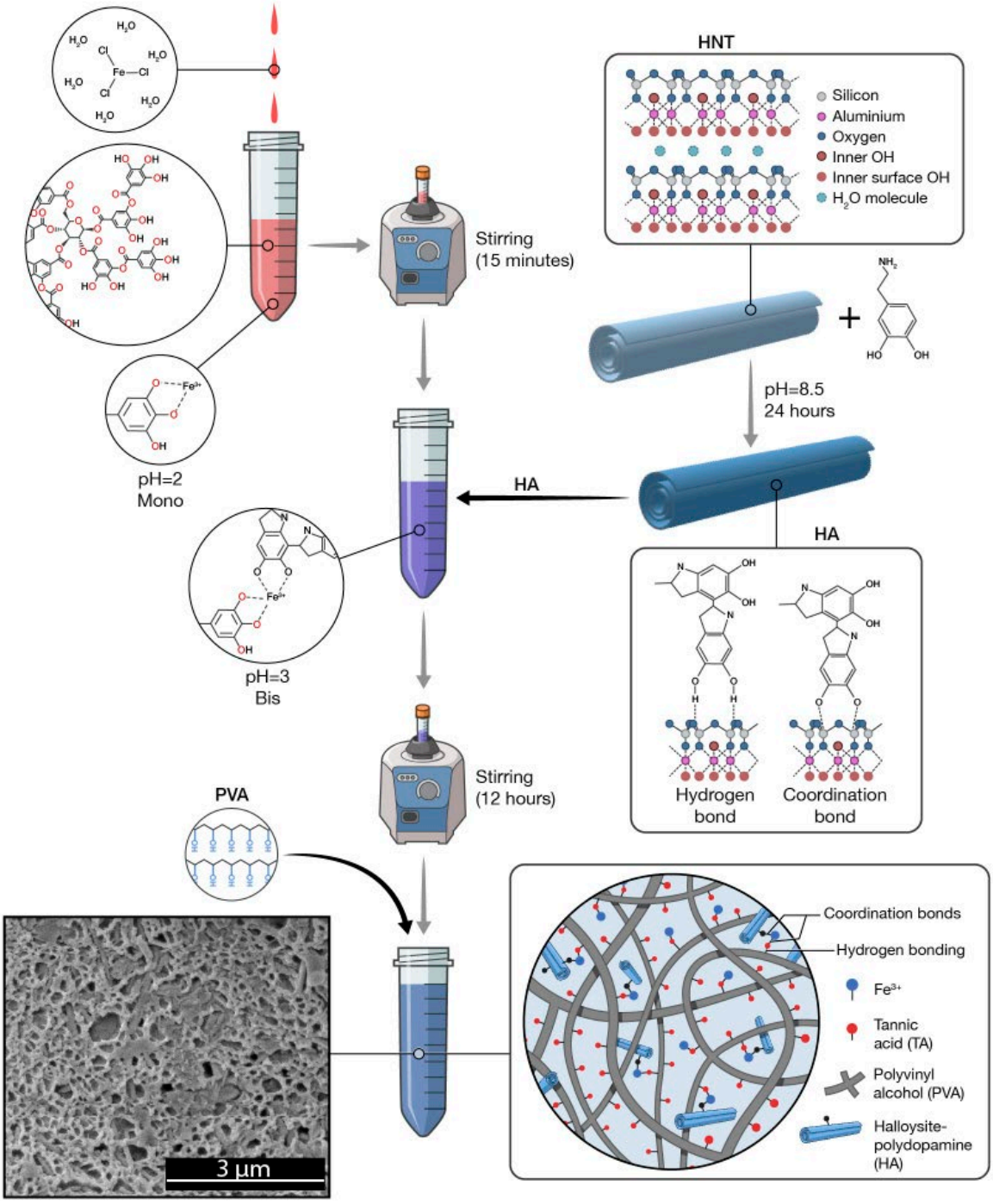

Figure 1. Schematic description of the CareGum (PATA-xHAF) synthesis process. Tannic acid and iron(III) chloride hexahydrate were mixed together forming a mono coordination complex at pH = 2. After 15 minutes of stirring, the required amount of HA hybrid nanocomposite was gradually added and stirred for at least 12 h to form a bi-coordination complex. Finally, PVA solution was added and mixed with spatula until PATA-xHAF formation was fully commenced.

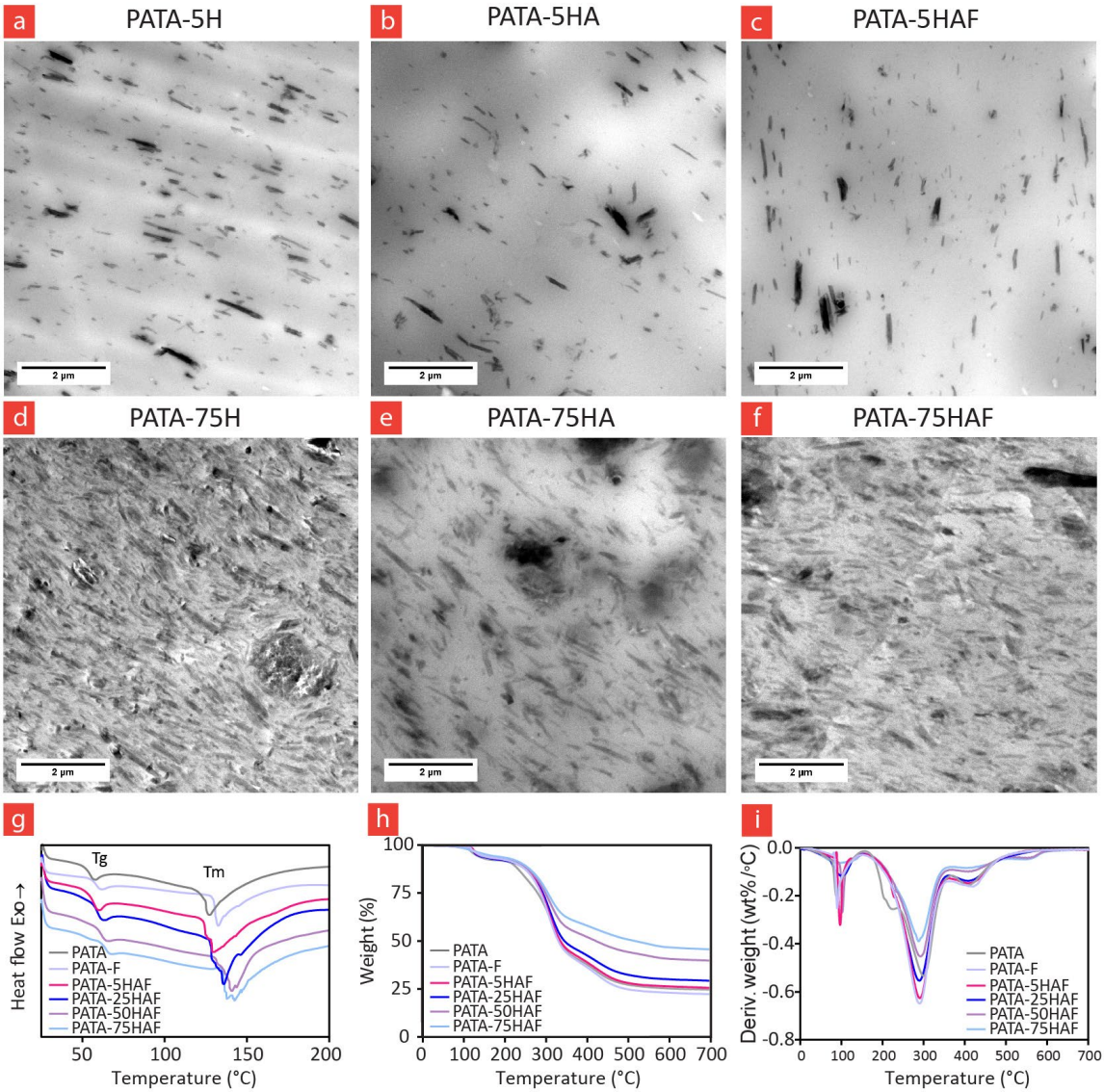

Figure 2. CareGum chemical Characterization. TEM images presenting the alignment of halloysite nanotubes (HNT) within (a) PATA-5H, (b) PATA-5HA, (c) PATA-5HAF, (d) PATA-75H, (e) PATA-75HA and (f) PATA-75HAF. (g) DSC analysis, (h) TGA analysis and (i) DTG analysis.

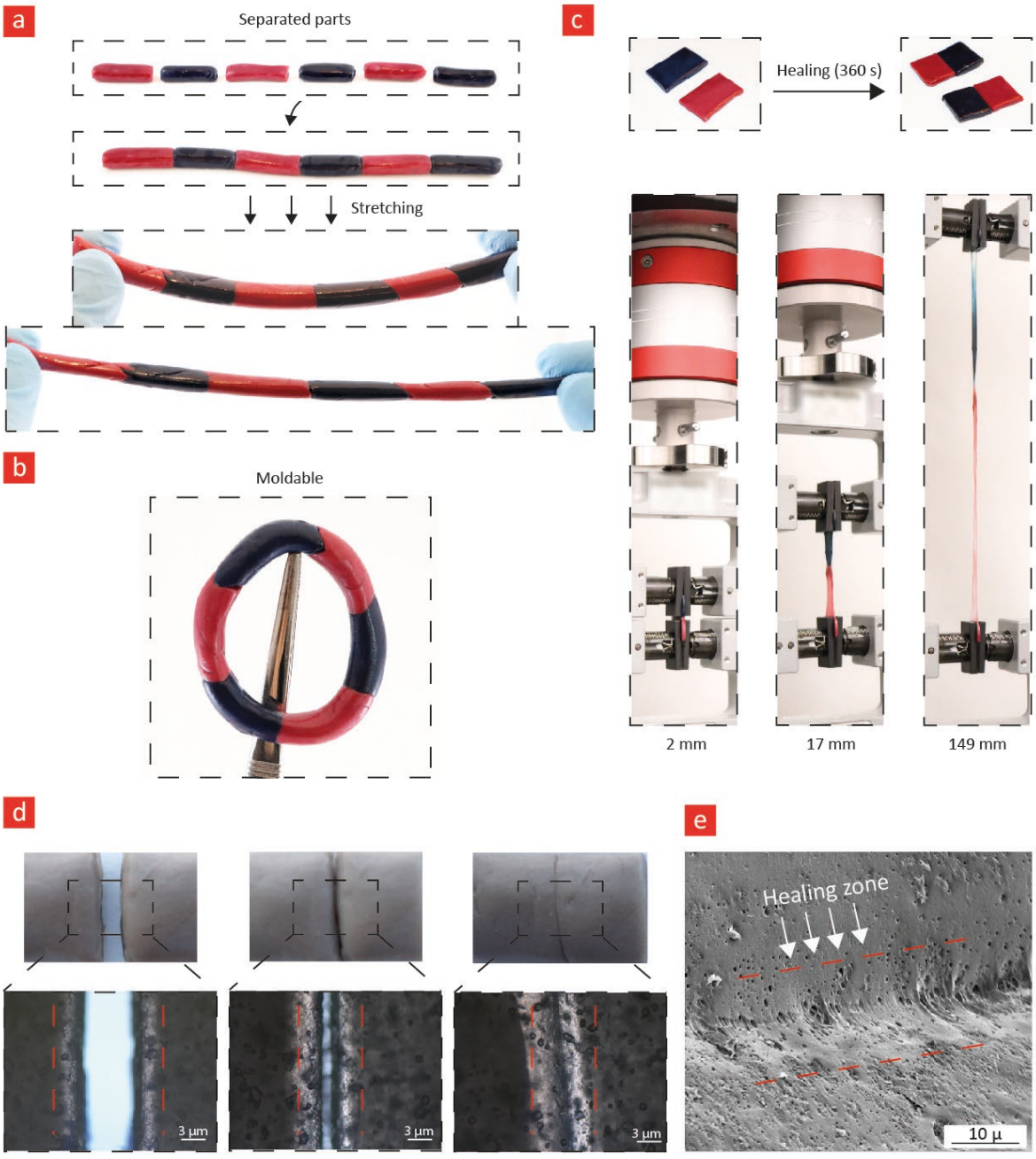

Figure 3. Remodelling studies. (a) CareGums loaded with red and blue dyes were prepared and cut into small pieces to showcase their self-healing, moldable and stretchable properties. As can be seen from the images, broken CareGum pieces were put together to facilitate rapid healing. It is also evident that the self-healed system remained flexible and (b) moldable. (c) The image shows that the composite maintains its high stretchability after the healing process. Indeed, it can be stretched 75 times its original length. (d) Photographs showing the healing process of a CareGum (PATA-F) on a microscopic level with optical microscopy and (e) SEM imaging.

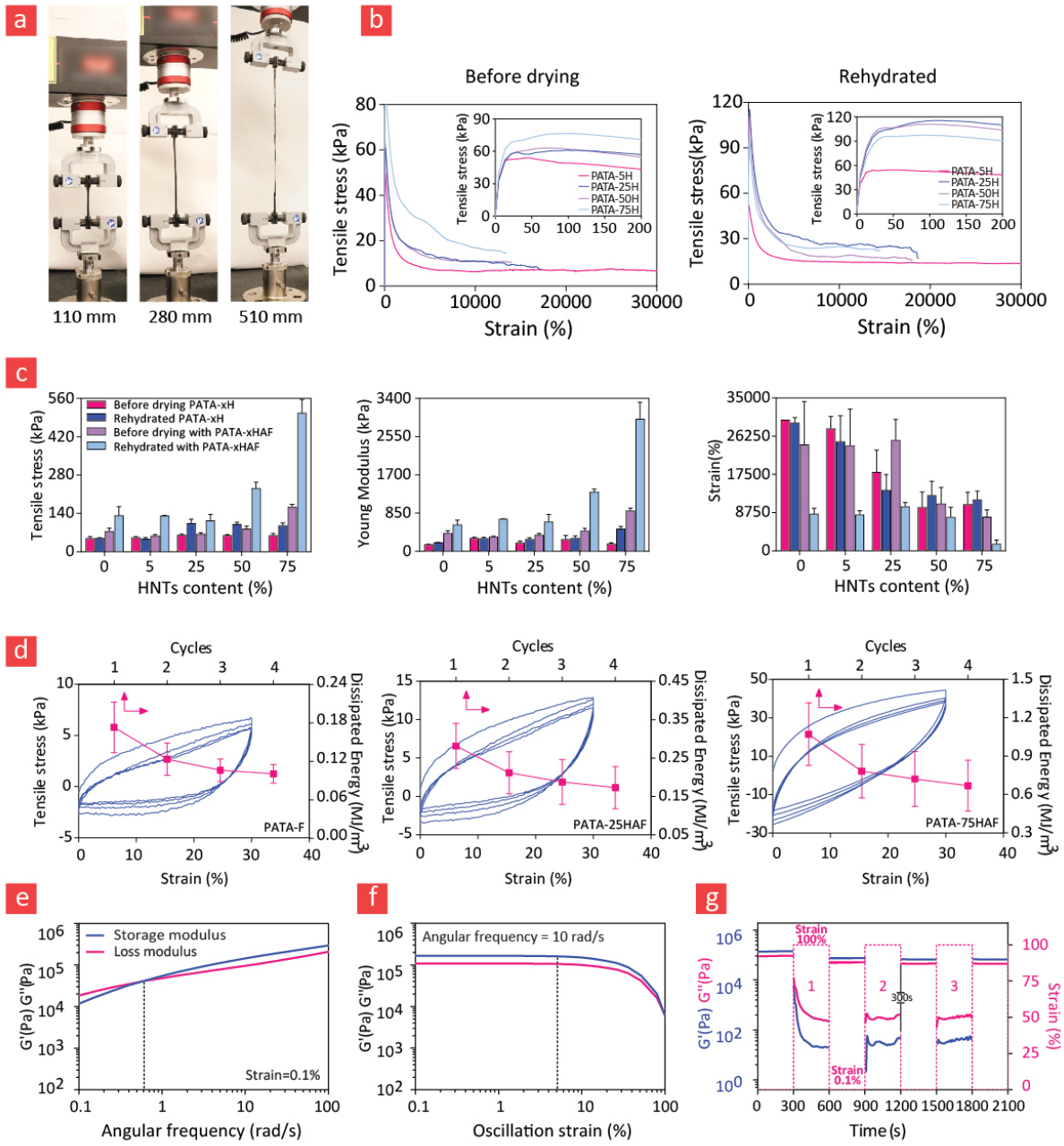

Figure 4. Mechanical analysis. (a) Images demonstrating the high stretchability of the PATA-75HAF CareGum (b) Stress-strain curves representing tested samples before drying and after rehydration. (c) Maximum tensile stress (tensile strength), Young's modulus and strain at breakage values for the various tested composites PATA, PATA-F, PATA-xH and PATA-xHAF. (d) Cyclic measurements and the corresponding energy dissipation values per cycle for PATA-F, PATA-25HAF and PATA-75HAF. Rheology experiments were also performed to examine the storage modulus G' and loss modulus G'' of PATA-75HAF with regards to (e) angular frequency and (f) oscillation strain. (g) The self-healing capacity of Caregums (PATA-75HAF) were also probed through rheology. All the rheology specimens were subjected to cycles of 0.1 % and 100 % strain with a recovery time of 360 sec.

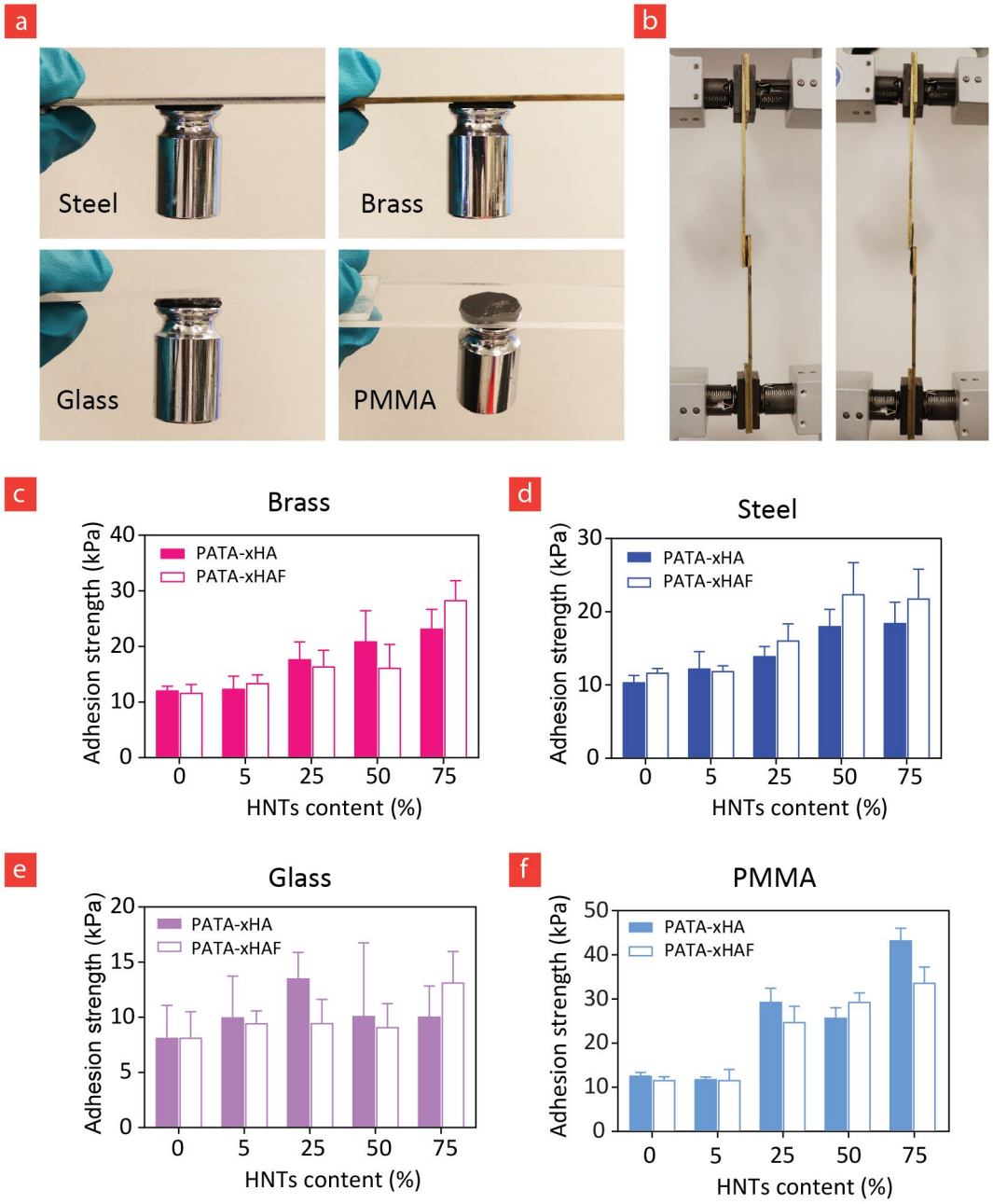

Figure 5. CareGum Adhesion. (a) Pictures showing the adhesive properties of PATA-75HAF composites to different surfaces including steel, glass, brass and PMMA. (b) Photographic images of the lap-shear testing setup. The Adhesion strength of PATA-xHA and PATA-xHAF composites on different surfaces including (c) brass, (d) steel, (e) glass and (f) PMMA was quantified with universal test machine Instron 5967 and are displayed here.

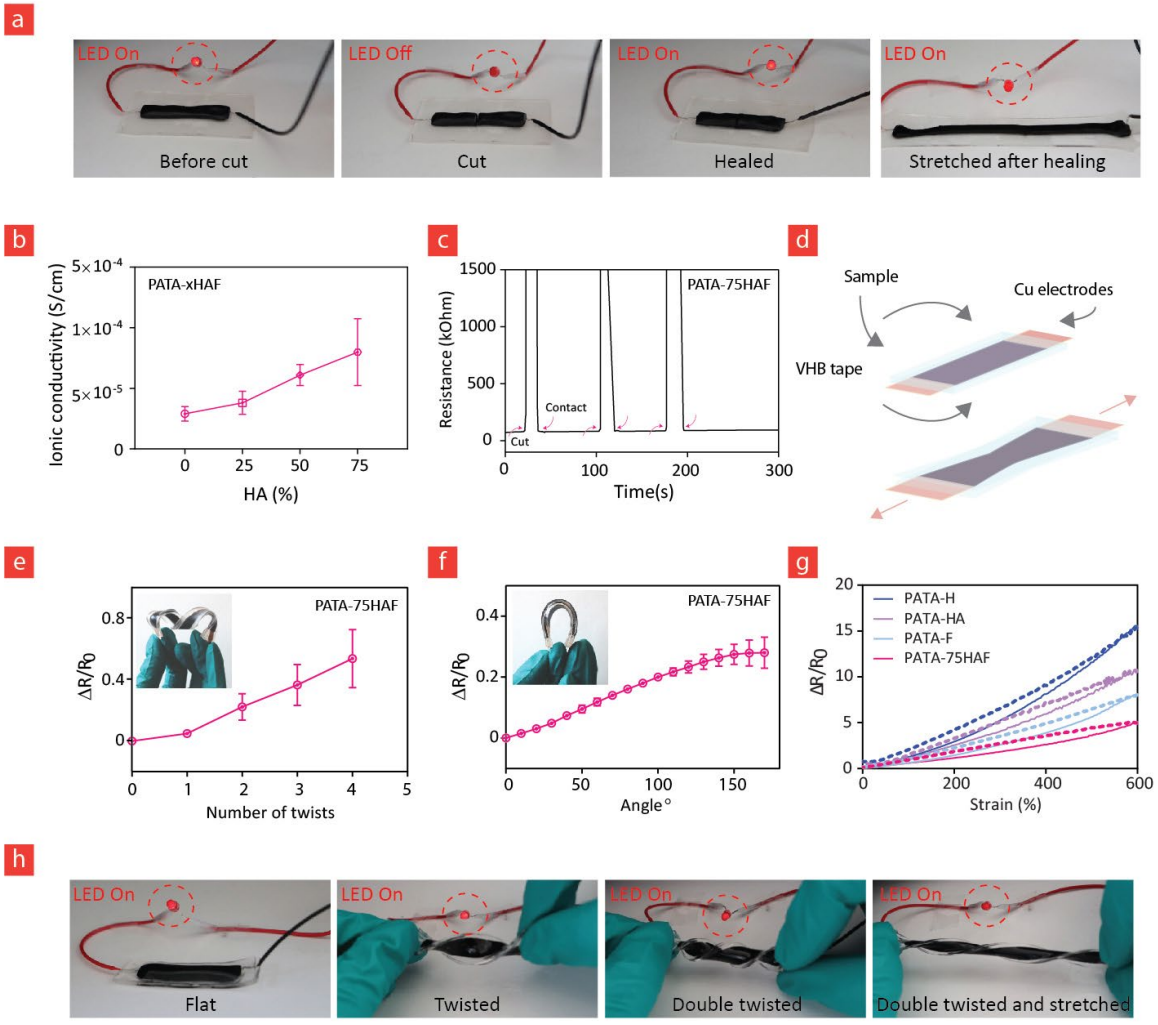

Figure 6. Electromechanical analysis. (a) Photographs showing the electrical healing capacity of CareGums (PATA-75HAF). In brief; a LED was attached to a PATA-75HAF CareGum strip and powered to illuminate. After cutting the circuit into separated parts, the LED stopped illuminating; however due to a rapid electrical self-healing capacity it started glowing almost immediately after the reconnection of the broken pieces. Notably, it could also stretch without compromising the glow from the LED. (b) Ionic conductivity measurements for PATA-xHAF CareGums as function of nanotube content. (c) The electrical self-healing capacity was examined by measuring the resistance change before and after broken PATA-75HAF CareGum pieces were reconnected. (d) An illustration showing the embedment of a CareGum within VHB tape. We did this to maintain stable electrical connections and to prevent unwanted drying of the encapsulated ionic conductor. Relative resistance change of PATA-75HAF CareGum due to (e) twisting, (f) bending and (g) comparison of PATA-75H, PATA-75HA, PATA-F and PATA-75HAF (g) straining. (h) Photographs of the LED response to applied twist and stretching with PATA-75HAF CareGum.

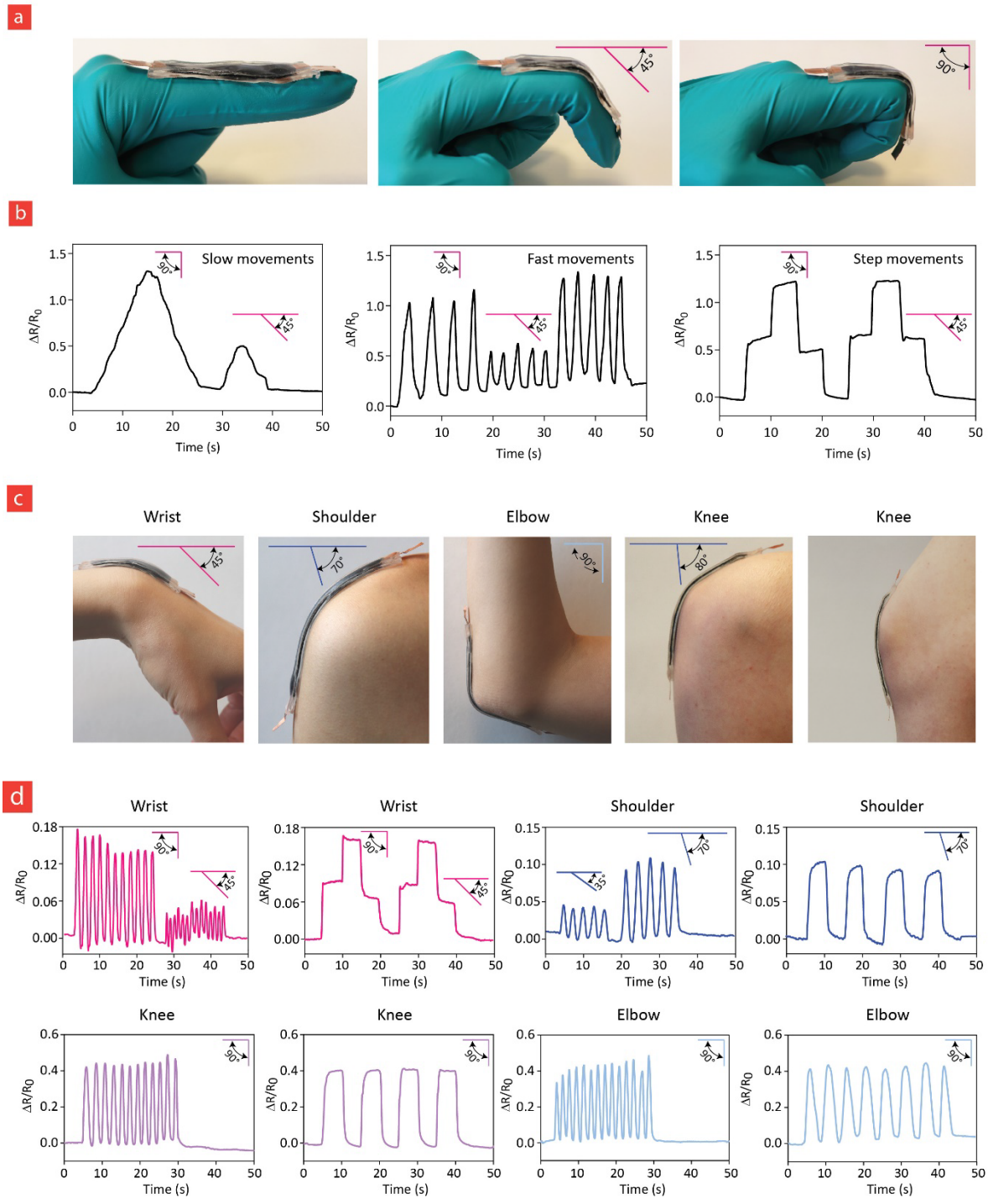

Figure 7. CareGum PATA-75HAF sensing properties. (a)– (b) Pictures demonstrating finger motion measurements. The relative resistance changed in a characteristic manner after slow, fast and step movements. (c) Pictures demonstrating that the CareGum sensor could attach firmly to wrist, shoulder, elbow and knee. (d) Relative resistance changes due to the movement of different parts of the human body. Notably, the CareGum could be used to monitor how fast the various tested body parts could move – as faster movements lead to more closely spaced relative resistance peaks.

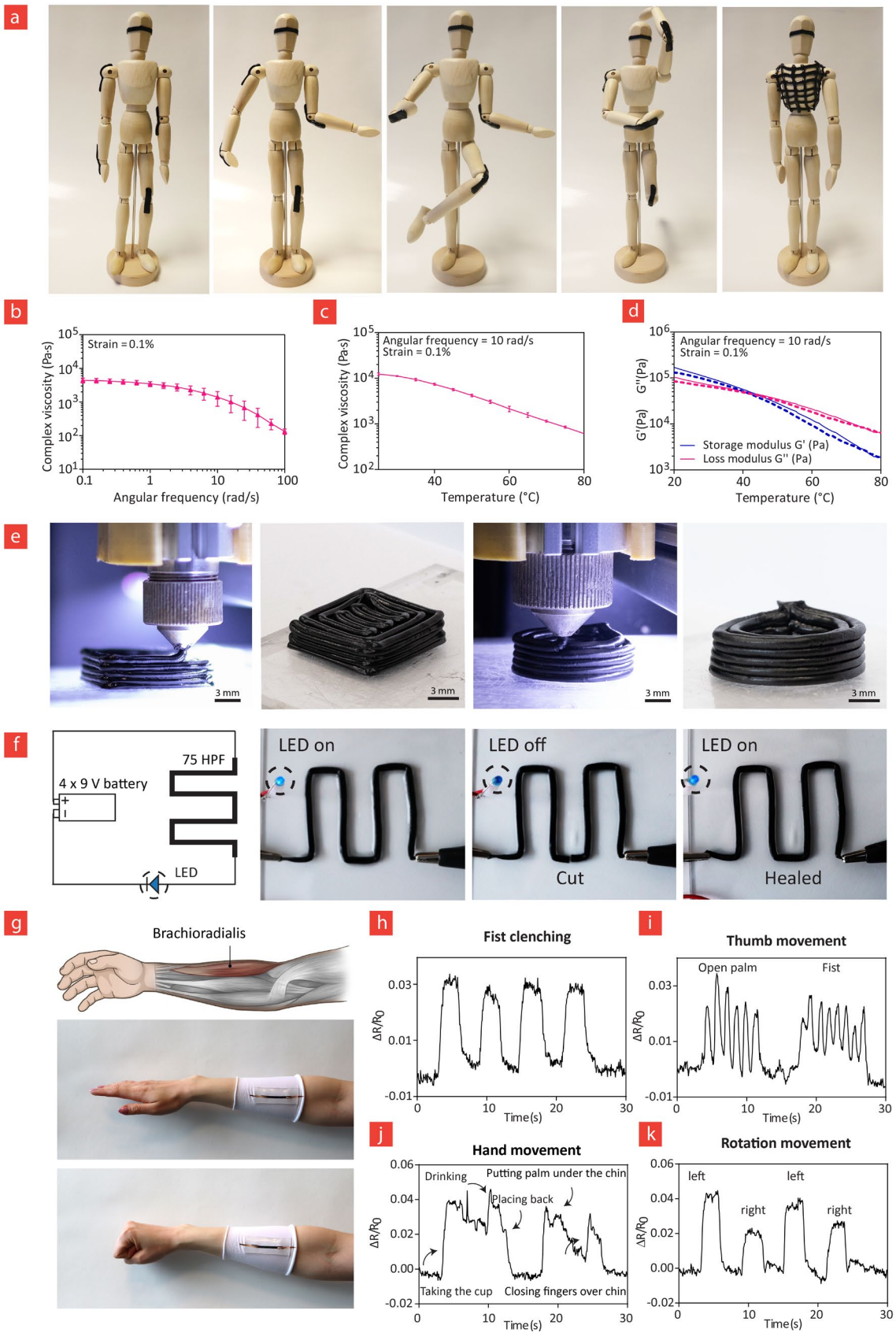

Figure 8. CareGum PATA-75HAF printability. (a) Images displaying the capacity of the CareGum to become custom-fitted on different parts of the curved and complex anatomy of a human figurine. Rheological experiments were performed in order to evaluate (b) shear thinning behaviour at 60°C in

frequency sweep mode, (c) complex viscosity change with increasing temperature and (d) cyclic moldability experiments to highlight the reversible behaviour of storage modulus G' and loss modulus G'' in response to cyclic temperature changes. (e) Pictures demonstrating that CareGums can be printed into complex 3D shapes and architectures through material extrusion 3D printing with 1.5 mm nozzle size. (f) Schematic description of the electrical circuit generated through 3D printing of CareGum and related images showing that printed circuits still exhibited a fast self-healing capacity. (g) Schematic of brachioradialis muscle and photographs demonstrating a sleeve made out of stretchable fabric onto, which a CareGum was 3D printed. A series of brachioradialis motion measurements corresponding to different hand movements including, (h) fist clenching, (i) thumb movement, (j) hand movement and (k) rotation movement.

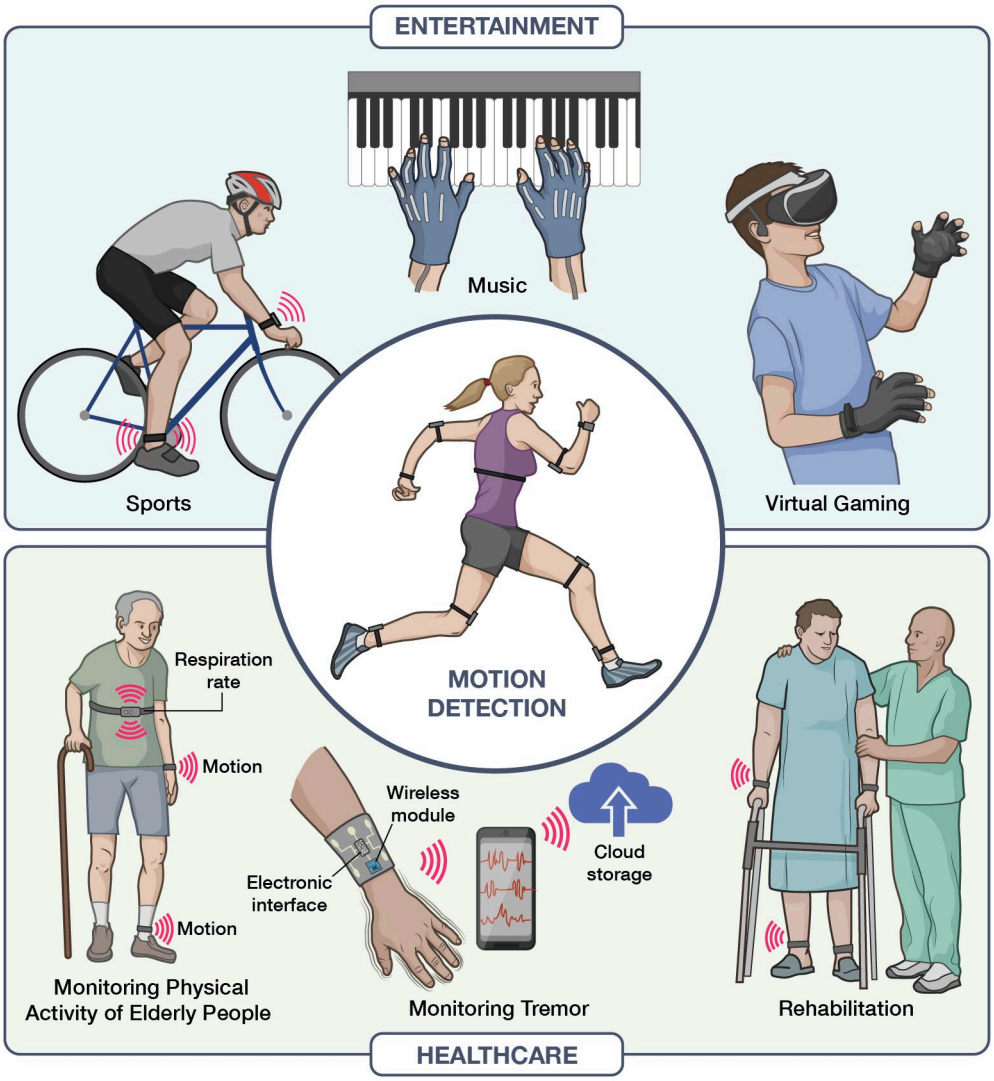

Figure 9. Motion plays an important role in our daily lives. It gives us freedom to move, to exercise and can increase our life-quality through full-filling activities such as sports, music and virtual gaming. However, motion detection is also important in healthcare. Indeed, patients undergoing rehabilitation need to perform strenuous exercises for a fast recovery. Wireless transmission of motion during such exercises can better help the physician and patient to optimize the exercises for an even faster recovery process. Finally, motion detection is important in the diagnostic and monitoring of various tremor-based diseases such as Parkinson's disease - and for monitoring the well being of the elderly; something intimately linked with their physical activity.

Table and caption

Table 1. Experimental values retrieved from DSC, TGA and DTG.

Sample	Tg (°C)	Tm (°C)	ΔH_m (J/g)	$T_{10\%}$ (°C)	$T_{50\%}$ (°C)	Residue (%)
PATA	55.07 ± 1.47	128.40 ± 1.73	129.25 ± 1.35	220.23 ± 0.39	333.35 ± 0.46	25.00 ± 0.14
PATA-F	58.47 ± 2.51	131.31 ± 4.04	98.67 ± 3.34	232.08 ± 0.15	330.38 ± 0.43	22.38 ± 0.16
PATA-5HAF	60.30 ± 1.08	132.85 ± 0.81	98.89 ± 3.92	235.47 ± 0.36	335.08 ± 0.08	25.22 ± 0.41
PATA-25HAF	61.28 ± 0.55	134.69 ± 0.89	95.98 ± 6.73	232.44 ± 0.25	345.04 ± 0.56	29.13 ± 0.31
PATA-50HAF	63.80 ± 0.75	138.84 ± 2.07	83.96 ± 9.22	238.12 ± 0.32	423.67 ± 0.31	40.44 ± 0.40
PATA-75HAF	66.35 ± 0.37	138.72 ± 3.73	82.56 ± 0.22	245.08 ± 0.12	520.42 ± 0.36	45.29 ± 0.06

Table of Contents

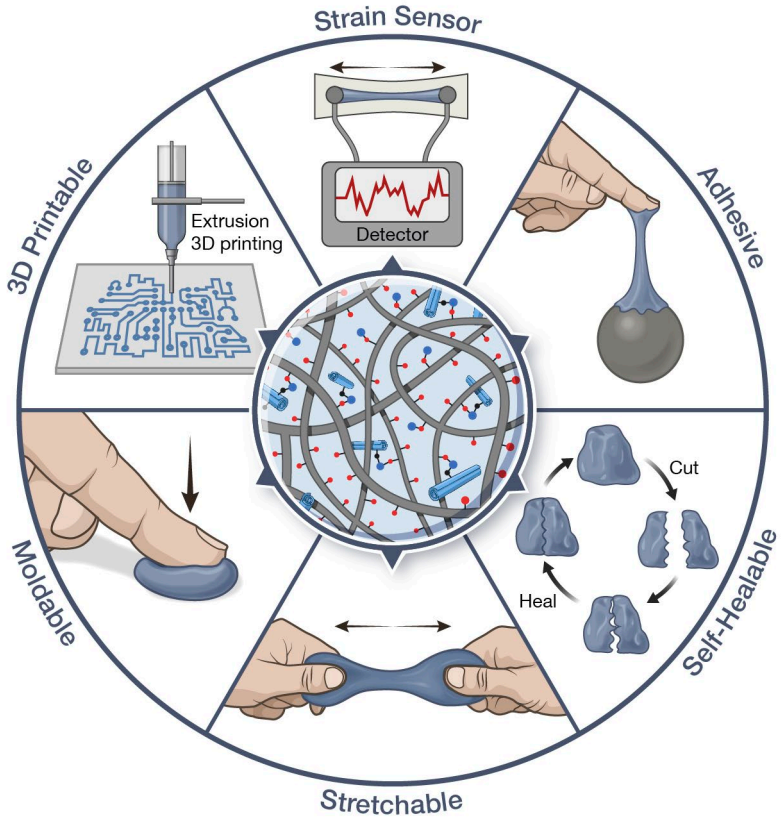

The wide range of properties that CareGum displays are illustrated here. It exhibited vast stretchability while being adhesive, 3D printable, self-helable and moldable at the same time. Notable, the CareGum was highly strain-sensitive and could maintain its electrical properties even after repeated mechanical cycles – a phenomenon related to the inclusion of electrically active nanotubes and subsequent alignment of these within the CareGum matrix.